VOLTAGE AND POWER CONTROL OF INVERTER-INTERFACED DISTRIBUTED GENERATION SYSTEMS USING COMBINED DIRECT CURRENT VECTOR CONTROL AND DROOP CONTROL METHOD

by

MALEK RAMEZANI

SHUHUI LI, COMMITTEE CHAIR
TIMOTHY HASKEW
S. NIMA MAHMOODI

A THESIS

Submitted in partial fulfillment of the requirements
for the degree of Master of Science
in the Department of Electrical and Computer Engineering
in the Graduate School of
The University of Alabama

TUSCALOOSA, ALABAMA

2016

ABSTRACT

In recent years, distributed generation (DG) systems have become a significant power source for remote areas and local loads. Almost all of the DG sources are inverter-interfaced to deliver the power to the loads in the desired form, which is *ac*. On the other side, most of the loads are very sensitive not only to changes in voltage levels and frequency of the power supply system, but also to harmonic distortion. Therefore, the use of diesel driven synchronous generators and similar power sources will be limited for many applications in the near future because of the high harmonic content of the output voltage when a non-linear load is applied. A solution to these limitations is to use an inverter to generate high quality sinusoidal voltages within a system which controls the instantaneous voltage.

Proliferation of distributed resource (DR) units in the form of distributed generation (DG) and distributed storage (DS) has brought about the concept of the microgrid. A microgrid is defined as a cluster of DR units and loads that can operate in a) the grid-connected mode, and b) the islanded mode. Proper operation of the microgrid in both the grid-connected and islanding modes requires the implementation of high-performance power flow control and voltage regulation algorithms. Grid-connected operation consists of delivering power to the local loads and to the utility grid. In the absence of the grid, the inverters are normally operated in the island mode, in which inverters are responsible for establishing the *ac* bus voltage and supplying a high quality power to the loads.

This research presents a novel control strategy for parallel operation of inverters within the distributed *ac* power supply systems. The proposed control technique, based on the droop control method, uses only locally measurable feedback signals. This method is usually applied to achieve good active and reactive power sharing when communication between

the inverters is difficult due to physical separation. To improve the voltage regulation and reactive power sharing, integrating the direct current vector control (DCVC) with droop method is proposed in this thesis.

DEDICATION

This thesis is dedicated to the memory of my mother. To the memory of my brother Dr. Hossein (Malik) Ramezani (1983-2011), my best friend, one day we will meet again. To my father who taught me to be patient and persistent. To my siblings who always give me encouragement. I will be forever indebted to them.

LIST OF ABBREVIATIONS AND SYMBOLS

AC	Alternative Current
CSI	Current Source Inverter
DC	Direct Current
DCVC	Direct Current Vector Control
DER	Distributed Energy Resource
DG	Distributed Generation
DR	Distributed Resource
DS	Distributed Storage
ESR	Equivalent Series Resistance
ISBS	Intelligent Static Bypass Switch
PCC	Point of Common Coupling
PI	Proportional Integral
PLL	Phase-Locked Loop
PV	Photovoltaic
RF	Reference Frame
RMS	Root-Mean-Square
SPWM	Sinusoidal Pulse Width Modulation
UPS	Uninterruptible Power Supply
VA	Volt Ampere

VAR	Volt Ampere Reactive
VSI	Voltage Source Inverter

ACKNOWLEDGMENTS

Firstly, I would like to express my sincere gratitude to my advisor Prof. Shuhui Li for the continuous support of my research, for his patience, motivation, and immense knowledge. His guidance helped me in all the time of research and writing of this thesis. I could not have imagined having a better advisor and mentor.

Besides my advisor, I would like to thank the rest of my thesis committee: Prof. Tim A. Haskew , and Dr. S. Nima Mahmoodi , for their insightful comments and encouragement.

CONTENTS

LIST OF TABLES

LIST OF FIGURES

1. INTRODUCTION

1.1. Parallel Inverters Applications

By increasing the dependency of nowadays societies to electrical and automation systems, providing the reliable power supply systems is a necessary task. For critical loads, such as, hospitals, telecommunication systems, etc., which the power outage will cause severe damages, this necessity is more sensible [1]. The current power systems, including generation, transmission, and distribution; also, are not able to provide the necessary reliability for these critical loads because of intentional or unintentional power outages in these systems.

In addition to reliability issue, the power quality has not reached yet to the desire level which could be suitable for modern and sensitive equipments. Besides, the increasing utilization of power-electronics converters based loads, computers, and the other sensitive electronic loads, has made the power quality issue one of the most important ones. The voltage drop issue is one of the most common disturbance which affects the power quality, insofar as, more than 92 percent of the disturbances causing power quality problem have been related to this issue.

The aforementioned issues make it necessary to utilize a backup power supply for the critical loads. The diesel generators and uninterruptible power supplies (UPS) are the option for such a systems. Nevertheless, the long startup time and the high harmonic contents in the case of supplying the nonlinear loads are the issues associated with diesel generators. Therefore, utilizing the UPS systems seems to be the best option to achieve the high reliability and power quality for supplying the critical loads.

Coordinated operation of the UPS systems with the main grid system will guarantee the continuity of the power to the critical loads. In normal operation the loads are supplied

by the main grid; upon, a power quality issue the loads will be disconnected from the grid and the UPS systems will take over the responsibility of providing power to the loads. The question, which usually arise with the application of UPS systems to supply the critical loads, is that if using a high capacity UPS is better or utilizing several UPS systems in parallel operation. The answer is that using of either has pros and cons; therefore, selecting each of these options depends on the degree of reliability, installation area, and the maintenance aspects. Usually, using an UPS with higher capacity may be is more cost effective than using several low rating UPSs [2]; however, using parallel UPSs will increase the reliability, flexibility in installation, maintenance, and even being expandable which are described as follows.

- **Reliability:** The parallel operation of inverters will increase the reliability, extensively. If one of the units fails the other units will guarantee the continuity of the power.
- **Expandability:** In the case if demanding power is higher than the capability of the current parallel structure, it will be possible to provide demanded power by adding extra UPSs to the parallel units.
- **Maintenance:** The maintenance of parallel units would be much simpler to be handle than the concentrated structure.

The most important issue associated with parallel operation of inverters is the complexity of their power control system. In parallel operations, the units should be controlled in such a way to prevent the overloading while providing a high power quality. Since the parallel units may be located at the different and far way locations, communicating the controlling signals will be an issue and may also degrade the reliability of the system; therefore, controlling the units should be based on the local data which would increase the complexity of the control system.

The application of parallel inverters is not just limited to the UPS systems, they are also applied to the distributed generation (DG) systems. Because of the environmental and economical advantages, developing and utilizing the green energy sources and DG systems

have gained more attention in the last few years. The main characteristics of the DG systems which make them more distinctive from the common power plants are their location and power rating. The power plants are usually connected to the high power transmission lines to deliver the power to the consumers. The DG sources, however, are usually located in a limited specific area and are connected to a local grid which is called Microgrid and close to the consumers. In such a system (microgrid) because of the high distance between DG sources each unit needs to operate independently from the other units while maintaining the voltage and frequency in an acceptable level and supplying the power proportional to their rated capacity.

Fig. 1.1 shows the overall structure of a microgrid including a few DG sources, distributed loads, and power electronics converters. The power electronics converters transfer the energy to the distributed loads and the grid. The inverters in microgrid basically operate in two different mode: the grid-connected mode and the islanding mode.

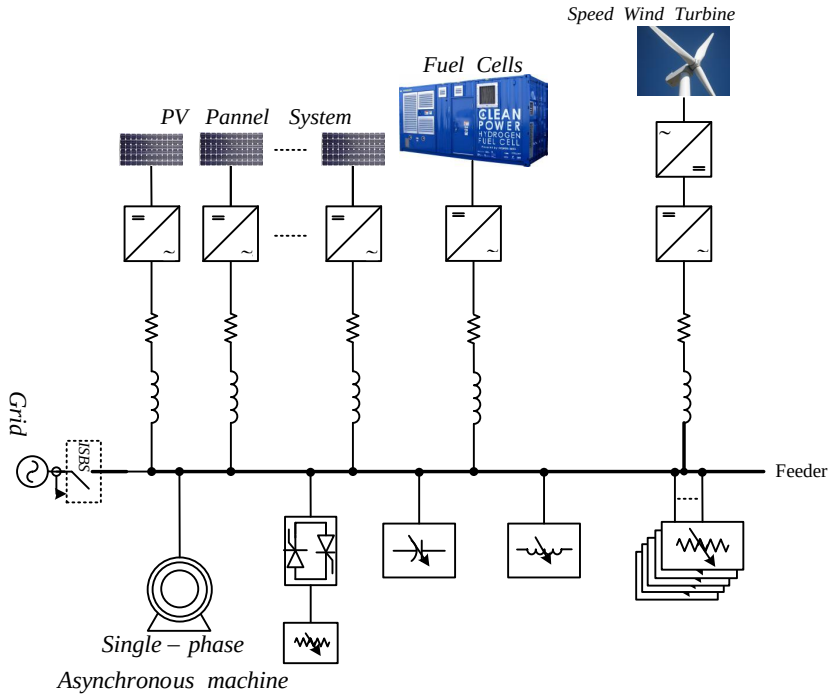

Figure 1.1: Overall structure of a microgrid.

In grid connected mode the DG sources will be controlled in such a way to provide constant power to the grid. In islanding mode which is investigated in this research, nevertheless, the DG sources will be controlled to keep the voltage and frequency in the acceptable range while providing the total demanded power to the loads. The islanding mode, basically, may occur by one of the following reasons:

- Maintenance which is called pre-scheduled islanding.
- Fault in the main grid, unscheduled islanding.

The islanding mode will be activated by opening the intelligent static bypass switch (ISBS), showing in Fig. 1.1. Upon disconnecting the microgrid from the main grid the DG sources are responsible for providing the demanded power and keep the frequency and voltage in the acceptable range.

The acceptable operation of a system which includes the parallel inverters requires four following major properties:

1. Providing the equal voltage amplitude, frequency, and phase angle at the output of each unit.
2. Sharing the load current between units based on their rated capacity.
3. Flexibility in increasing the number of units.
4. hot-swap operation ability

The hot-swap means the possibility of the plug in and out of each inverter without significant disturbance in output current of the other units and in the power quality of the microgrid. Therefore, the designed control system should satisfy the above mentioned properties.

1.2. Control Methods of the Parallel Inverters

There are four types of control methods for power control of inverters in parallel operation as follows:

1. Instantaneous current sharing using master/slave method.

2. The deviation from average active/reactive powers method.
3. Frequency and voltage droop method.
4. Harmonic and reactive currents injection method.

1.2.1. Instantaneous Current Sharing Using Master/Slave Method

In order to share the identical power between parallel inverters, the instantaneous current sharing technique utilizes the load current as the feedback signal to the parallel units. In this method one of the inverters operates as the master unit which provides and stabilizes the required voltage for the load, and the other units tries to inject the same current in their output as their feedback load-current signal, these unites operate as slave controllers [3]. Fig. 1.2 shows the block diagram for this control method [4].

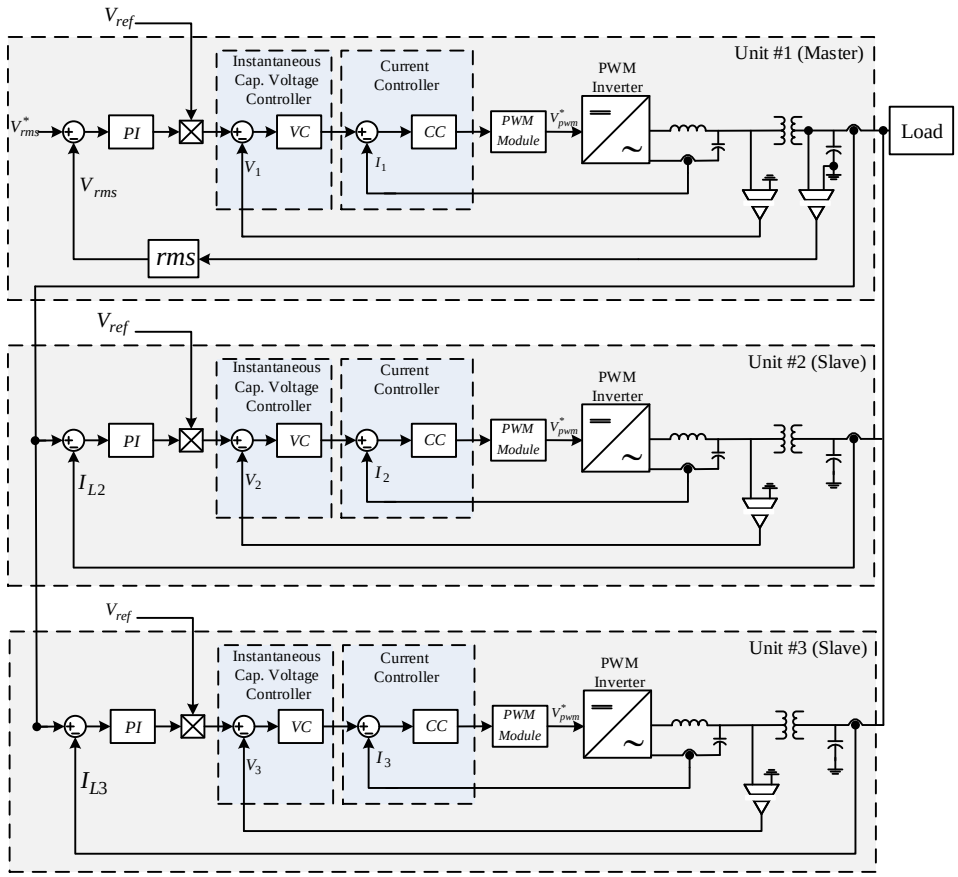

Figure 1.2: Master/slave control method, type 1.

As it can be seen in Fig. 1.2, each unit consists of a pulse width modulation (PWM) inverer following by an LC filter and a transformer, a voltage control, and a current control loop. The unit number 1 operates as master unit and stabilizes the required load voltage based on the reference voltage . In UPS applications, usually, the reference voltage is synchronized with either an existence voltage, like grid voltage, or the controller internal oscillator. The outer rms-voltage control loop in master inverter regulates the load voltage, and the reference voltage amplitude is tuned by a PI controller. The output current generated by the master unit is feeded back to the slave inverters, then, the slave units try to regulate their output current equal to the feedback current signal using an outer current control loop as shown in Fig. 1.2. Note that in order to generate the synchronous voltages at the output of all inverters, in Fig. 1.2 the voltage reference is applied to the all units. This means all the units need to be equipped with a phase-locked loop (PLL) to synchronize the output voltage of each unit with the reference voltage.

The proposed method in [5] eliminated the necessity of using PLL in master/slave technique, by utilizing the current source inverters (CSI) as slave units. Fig. 1.3 shows the proposed control structure.

As it can be seen in Fig. 1.3, the master unit is a voltage source inverter (VSI) which is equipped with a simple voltage control loop. As it is mentioned before, this unit provides and stabilizes the required load voltage. The slave units are the current source inverters (CSI) which their reference current is generated by a module called power distribution center. This module measures the total load current and generates the reference current signals for slave inverters proportional to their rated capacity. Then, each slave unit regulates its output current according to the received reference current signal from power distribution center.

The main advantage associated with instantaneous current sharing method is the momentary load sharing between parallel units. No need to the load current measurement (type 1) is the other advantage which facilitates the expanding and developing of the system.

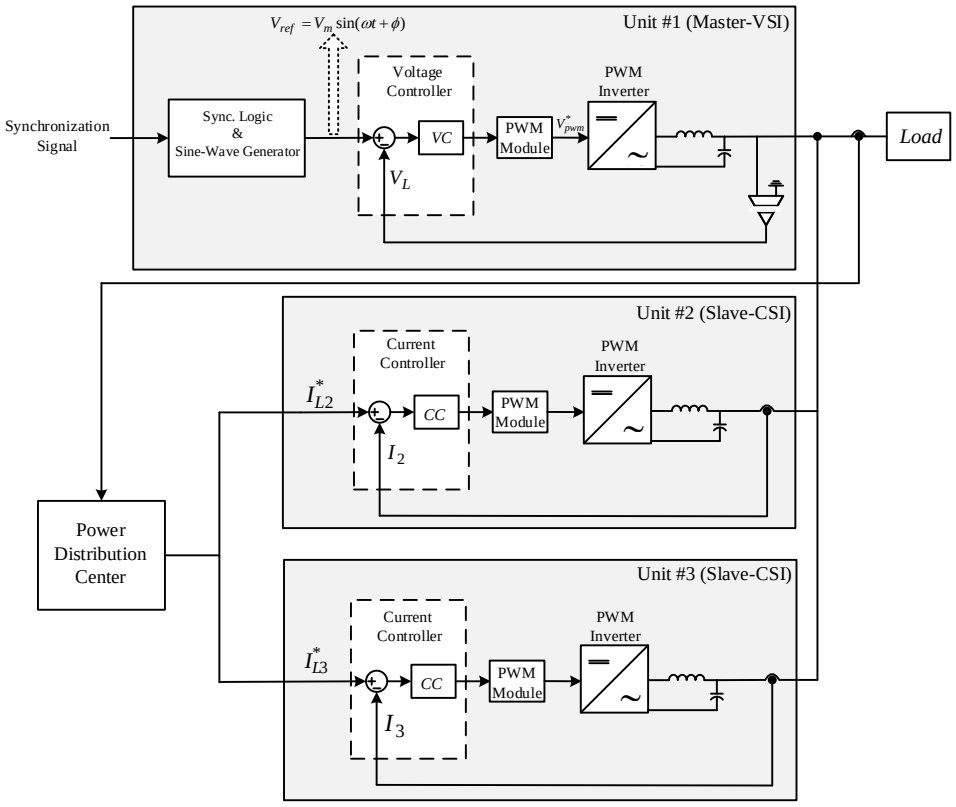

Figure 1.3: Instantaneous load sharing using master/slave control method, type 2.

The last but not the least, in this method the transmission lines will not affect the load sharing between inverters.

In the case of fault occurrence in the master unit the whole system will be out. Therefore, the requirement of a unit as the master unit is one of the major weakness of this method which degrades the reliability of the system. Recently, it is tried to enable the control system to replace the master unit with one of the slave unites in the case of fault in master unit to increase the reliability of the system and to keep the continuity of the power transferring. It is obvious this approach will increase the complexity and the cost of the control system comparing with common master/slave method. Moreover, the physical wiring between parallel units is the other weakness of this system which also declines the system reliability.

1.2.2. The Deviation From Average Active/Reactive Powers Method

This power sharing technique is designed based on the AC systems power flow theory, in which the transmission lines are considered dominantly inductive; therefore, the active power flow and reactive power flow will be a function of phase angle and voltage, respectively [6]. Fig. 1.4 shows the parallel connection of two inverters through different transmission line to a common load. The transmission lines are assumed inductive for simplicity.

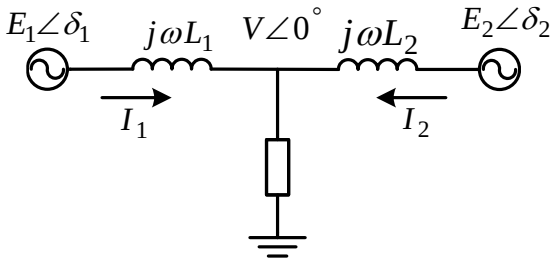

Figure 1.4: Parallel connection of two inverters to a common load.

The apparent power injected to the load by the inverter number 1 can be expressed as

$$S_1 = P_1 + jQ_1 = V.I_1^* \tag{1.1}$$

where I_1^* is the complex conjugate of the first inverter current, defining by the following equation.

$$I_1^* = \frac{E_1 cos\delta_1 + jE_1 sin\delta_1 - V}{j\omega L_1} \tag{1.2}$$

Substituting (1.2) in (1.1) results in (1.3)

$$S_1 = V.\left[\frac{E_1 cos\delta_1 + jE_1 sin\delta_1 - V}{j\omega L_1}\right]^* . \tag{1.3}$$

From (1.3) the active and reactive power injected by the inverter 1 to the load can be resulted as following.

$$P_1 = \frac{VE_1}{\omega L_1} sin\delta_1 \tag{1.4a}$$

$$Q_1 = \frac{VE_1 cos\delta_1 - V^2}{\omega L_1} \tag{1.4b}$$

Similarly, for the second inverter

$$P_2 = \frac{VE_2}{\omega L_2} sin\delta_2 \tag{1.5a}$$

$$Q_2 = \frac{VE_2 cos\delta_2 - V^2}{\omega L_2}. \tag{1.5b}$$

It can be concluded from (1.4) and (1.5) that if δ_1 and δ_1 are small enough, the active power flow will be dominantly affected by the power angles, δ_1 and δ_2; whereas, the reactive power flow is dominantly dependent on the output voltage of the inverters, E_1 and E_2. This denotes that the active and reactive power can be almost controlled independently.

Fig. 1.5 shows the block diagram of the deviation from average active/reactive power control method for two parallel inverters. Each inverter regulates its output active and reactive power, by tuning its internal voltage reference, to be equal to the average value of active and reactive power, respectively. To do so each inverter needs the active and reactive power values of the other unit to evaluate the average values. In [7] the active and reactive power of each unit is evaluated by dissection the load current to its active and reactive components.

Another aproach is proposed in [8], in which to provide a reference for the output current of each unit, the load current is divided over the number of units, then, the deviation of the output current of each unit from the outcome of the division is used to calculate the difference of active and reactive power from the average power. Finally, the active power deviation from the average is used to regulate the voltage phase angle and the difference between reactive power and the average value is used to tune the voltage amplitude. Fig. 1.6 depicted the control block diagram of this approach.

Since in this power control method there is no need for master unit, the reliability of the system is higher than the master/slave technique. Moreover, the accurate active and reactive power sharing between inverters in this method results in a lower circulation currents between units.

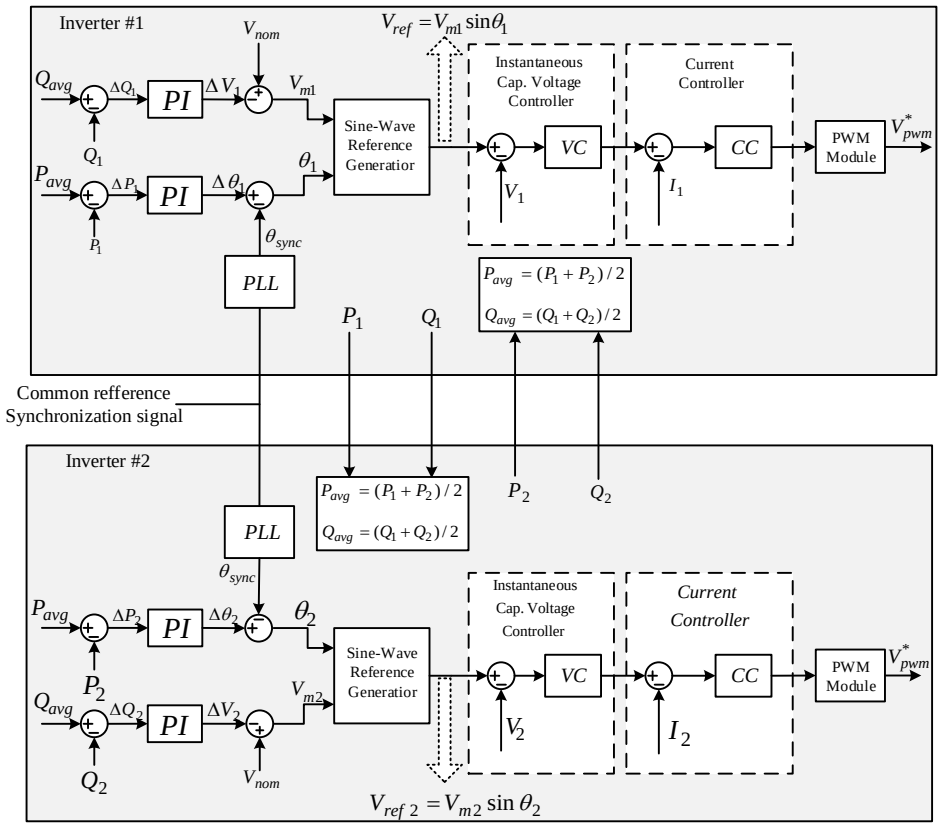

Figure 1.5: Deviation from average active/reactive power control method.

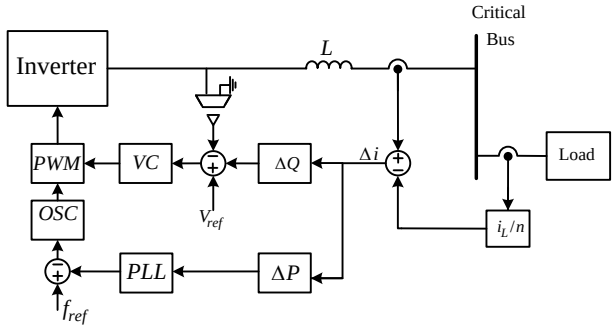

Figure 1.6: Block diagram of power deviation control.

One of the weakness of this method is that this approach affects only the fundamental component of the load current. Therefore, in the case of nonlinear loads this method would not be able to share the harmonic current between the inverters. The other weakness associated with this method is the communication link between units which deteriorates the system reliability.

1.2.3. Frequency and Voltage Droop Method

This technique employs the same concept as the multiple generators in power system take over the load sharing. The main idea of this method is the mimicking of the synchronous generator governor behaviour. In power systems, the synchronous generators share the change in load by the frequency drop, proportional to their governor droop characteristic. This makes it possible for synchronous generator to react to the load changing in a predetermined manner and utilize the system frequency as the communication link [9].
The droop technique is applicable to the parallel inverters by frequency and voltage amplitude drop at the output of the inverters proportional to active and reactive power, respectively. Note that in this technique the transmission lines are considered dominantly inductive.
In droop control method the $P-\omega$ (Active power - Frequency) and the $Q-V$ (Reactive power - Voltage amplitude) droop characteristics for a system including several inverters are expressed as follows [10]:

$$\omega_i = \omega_0 - m_i P_i \tag{1.6}$$

$$V_i = V_0 - n_i Q_i \tag{1.7}$$

where ω_i and V_i are the angular frequency and voltage amplitude of the ith inverter respectively, and the ω_0 and V_0 are the nominal angular frequency and voltage amplitude. m_i and n_i are called droop coefficients. Fig. 1.7 shows the block diagram for the frequency and voltage droop technique.

In order to share the power between parallel inverters proportional to their rated capacity, the droop characteristics slope need to obey the following rules

$$m_1 S_1 = m_2 S_2 = ... = m_n S_n \tag{1.8}$$

$$n_1 S_1 = n_2 S_2 = ... = n_n S_n \tag{1.9}$$

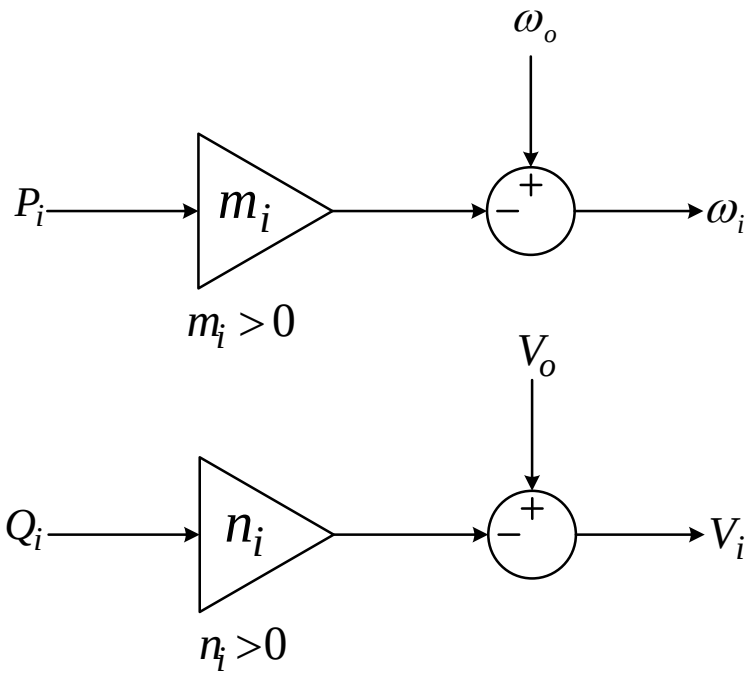

Figure 1.7: Frequency and voltage droop technique.

where S_i is the ith inverter rated capacity.

Fig. 1.8 shows the droop characteristics for two inverters which share the active and reactive power proportional to their rated capacity.

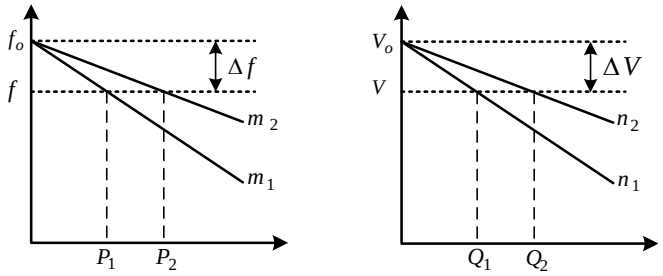

Figure 1.8: Droop characteristics.

the advantage of the droop control method is lack of the communication link for control signals which results in higher reliability for the system. Moreover, the maintenance of the system is feasible without any problem for the system. This control method, however, suffers from several weaknesses.

1. System frequency and voltage amplitude drop: Because of the droop characteristics, the system frequency and voltage amplitude drops so all the inverters operate at the lower frequency and voltage than rated values.
2. Lack of the ability to share the harmonic currents.
3. High sensitivity to the transmission lines: On of the weakness associated with droop method is that if the summation of the inverter output impedance and the transmission line impedance are not equal for parallel inverters the power sharing between units would face the obstacle. forasmuch as the DG sources are located at the different locations of the grid, these units are connected through the transmission lines with different length. this causes the inequality in transmission lines impedance and affect the load sharing between units, considerably.
4. Slow dynamic response: The dynamic response of the system consisting of parallel inverters is dominantly affected by droop coefficients, output impedance of the inverters, and the low-pass filters employing to filter out the average value of the active and reactive power of each unit. The low-pass filters decreases the bandwidth of the control system and consequently the system dynamic response is slow. Besides, the droop coefficient affects the accuracy and the speed of the load sharing, directly. The higher droop coefficients the higher accuracy and speed of load sharing would be; however, the power quality would deteriorate. The droop coefficients selection is a function of system rated frequency and voltage, rated output active and reactive power of the units, and the standard limits for frequency and voltage deviation. Therefore, the system dynamic cannot be improved independently, by using the droop method. It worth to note that the standard limits for frequency and voltage deviation are 2 and 5 percents, respectively [11].

Some techniques to minimize the droop method weaknesses have been proposed in literature. To improve the reactive power control in the case of imbalance lines impedance the virtual impedance technique is proposed [12, 13]. Adding the factorized derivative term

of the active and reactive power to the conventional droop terms to improve the transient response of the system is suggested in [14]. In [15] adding a large inductance in series with each inverter to improve the harmonic power sharing is proposed.

The active and reactive power sharing between parallel DG sources within a microgrid is proposed in [16]. In addition, the dynamic performance of the system, by extracting the small signal model of the system, is also studied in [17, 18], the weakness of the proposed approach is the lack of harmonic power sharing. [19] proposes to extract the harmonic components of the load current then a factor of this harmonic components is subtracted from the reference voltage to help the harmonic power sharing, the weakness of this method is the degradation in output voltage quality.

1.2.4. Harmonic and Reactive Current Injection Method

The injection signal approach proposing in [20] makes it possible to share the harmonic and reactive power between parallel inverters. In this technique two signals with the frequencies different from fundamental frequency is injected to the reference voltage, in which one of them is for controlling the disturbance power and the other helps to control the reactive power. It is noteworthy that the active power sharing in this approach is similar to droop control method. The voltage reference is

$$v_{ref} = \sqrt{2}(V cos\omega t + V_{h1} cos\omega_q t + V_{h2} cos\omega_d t) \tag{1.10}$$

where (V ω) are the system voltage and frequency, (V_{h1} ω_q) are the voltage and frequency of the injected signal corresponding to reactive power control, and (V_{h2} ω_d) are the voltage and frequency of the injected signal for sharing the harmonic power. Notice that V_{h1} and V_{h12} are constant; however, to control the harmonic and reactive power ω_d and ω_q are variable.

To share the reactive power, ω_q is dropped as a function of harmonic power as follow.

$$\omega_q = \omega_{q0} - b_q Q \tag{1.11}$$

Sharing the unequal reactive power will cause a difference between the frequency of the injected signals for differen units, which consequently will cause the phase difference between units. A small current, resulting from phase difference, flows in the reactive frequency which will also cause an active power in the same frequency (p_q), this active power could be used to tune the the voltage of the system. on the contrary of droop technique the system voltage in this method is supported as a function of (p_q).

To clarification, assume two units with Q_1 and Q_2 as their output reactive power, then the frequency of the injected signals by the units are

$$\omega_{q1} = \omega_{q0} - b_{q1} Q_1 \tag{1.12}$$

$$\omega_{q2} = \omega_{q0} - b_{q2} Q_2. \tag{1.13}$$

In this conditions, the frequency difference from the unit 1 point of view is

$$\Delta\omega_1 = \omega_{q1} - \omega_{q2}. \tag{1.14}$$

This frequency difference results in the phase difference, which cause an active power flowing as

$$\delta_1 = \int \Delta\omega_1 dt \tag{1.15}$$

$$p_{q1} = \frac{1}{X} sin\delta_1. \tag{1.16}$$

Where X includes the output impedance of the inverter and the transmission line impedance. This active power is used to support the reference voltage of the inverter.

$$V_1 = V_0 + b_v p_{q1} \tag{1.17}$$

where b_v is called the voltage support coefficient.

Now, assume $Q_1 > Q_2$ which results in $\omega_{q1} < \omega_{q2}$; therefore, $\Delta\omega_1$ is negative and makes the p_{q1} to be negative. Consequently, the amplitude of the output voltage of the inverter 1 drops. On the other side, $\Delta\omega_2$ and as the result p_{q2} would be positive which with the same reasoning causes the increase in the voltage amplitude of the second inverter and its output reactive power. This process will continue until two units reach the same reactive power in their outputs.

Similarly, for harmonic power sharing the ω_d is dropped as a function of the harmonic power.

$$\omega_d = \omega_{d0} - b_d D \tag{1.18}$$

where D is the harmonic power calculating using following equation

$$D = \sqrt{S^2 - P^2 - Q^2}. \tag{1.19}$$

As the reactive power case, here also a small active power, resulting from injected harmonic current with the frequency of ω_d, flows (p_d). This active power signal is utilized for tuning the bandwidth of the voltage control loop.

$$BW = BW_0 + b_w p_d \tag{1.20}$$

Fig. 1.9 shows the overall block diagram of the current injecting method. The main feature of this method is sharing reactive and harmonic power; besides, there is no need

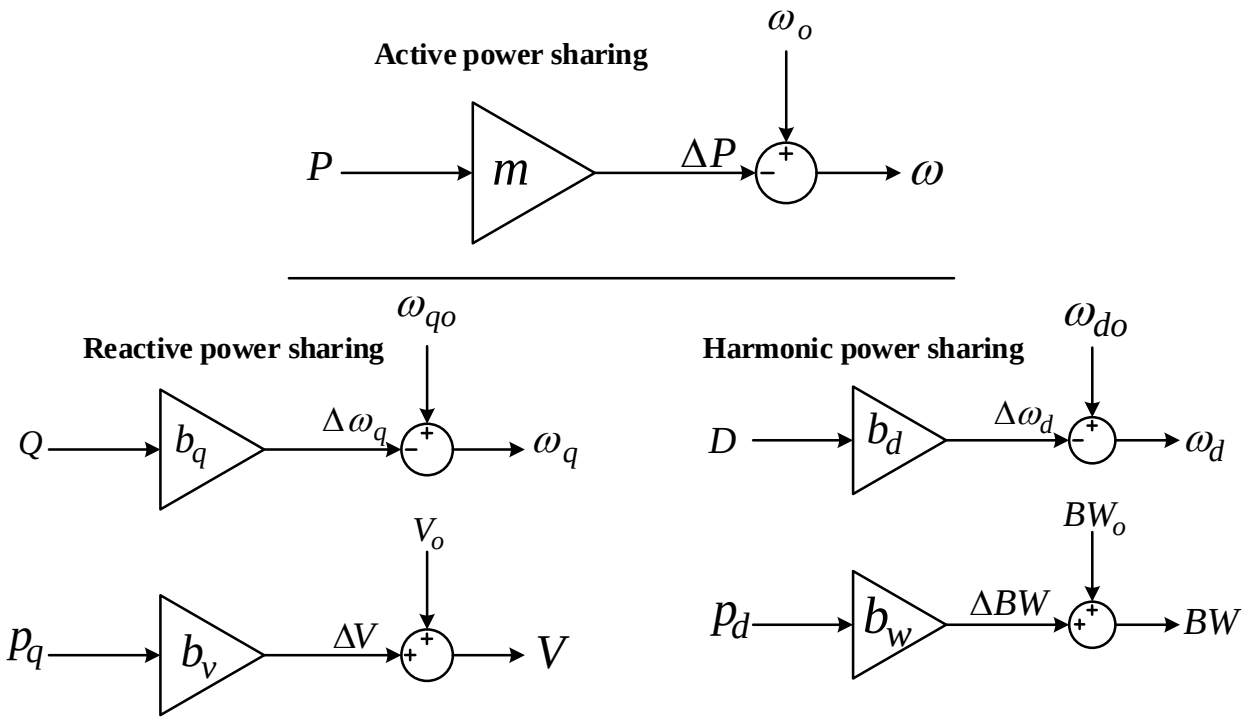

$$v_{ref} = \sqrt{2}(V\cos\omega V + V_{h1}\cos\omega_q t + V_{h2}\cos\omega_d t)$$

Figure 1.9: Load sharing using signal injecting method.

for control signals transmission between different units. On of the weakness inherent in this method is the inverter output voltage quality degradation, resulting from the injected signals. Moreover, the harmonic currents sharing is in the cost of system stability reduction (reduction in bandwidth). Utilizing the high frequency signals in this approach limits its application to low power inverters, where the switching frequency is higher. In high power inverters the switching frequency is lower and subsequently the LC filters with lower cutoff frequency are used; therefore, the high frequency signals, controlling harmonic and reactive powers, may affect the output of the units.

1.3. Research Motivation

The main aim of this thesis is to design a power control system for parallel inverters within a distributed *ac* power supply system. Since in designing the control system it is assumed that the transmission of control signals between units is not possible, the droop

methodology is selected as the power control system. As it is mentioned before, one of the issues associated with conventional droop method is the reactive power control and the sensitivity of the droop control system to the transmission lines impedance. Besides, the voltage drop associated with conventional droop control method is also one of the greatest weakness of this control approach. In this research it is tried, by integration the direct current vector control (DCVC) with conventional droop method, to deal with the reactive power control and bus voltage control issues simultaneously.

1.4. Thesis Organization

Nested control loops system for stand-alone inverter is responsible for current and voltage regulation of the inverter-interfaced DG system. This control system affects the inverter output impedance characteristic, significantly. In the next chapter the nested-control loops system is designed for the inverter. Since the power sharing and control among the parallel inverters is directly affected by the output impedance and transmission line impedance and in conventional droop based power control system the main assumption is based on the inductive impedances; therefore, in control system design the inductor current and capacitor voltage are chosen as the control signals to introduce an inductive impedance on the output of the inverter.

There are some weaknesses associated with conventional droop method such as reactive power sharing and voltage drop associated with reactive power sharing. The third chapter presented a direct current vector control (DCVC) method as the inner control loop for the inverter control system, and by integrating bus voltage control and droop based active power control as the outer control loops to the inverter nested control loops system, tries to solve the aforementioned issues of the conventional droop control method. Integrating the converter physical constraints within its control system is also one of the DCVCS strengths aspects.

Since the basic assumption in DCVC implementation is based on the grid-connected converter, in parallel inverters structure which is investigated in chapter 4 one of the inverters

is considered as a grid-forming inverter. The power control system for grid-forming inverter is based on the conventional droop method. The secondary active power control level is also integrated with droop and DCVC control techniques in this chapters to improve the power sharing accuracy and frequency control of the system. This chapter ended with dynamic performance evaluation of the droop control system and the simulation and hardware results analysis.

The last chapter (chapter 5) gives a conclusion for this thesis and suggests some research improvements for this work as the possible future researches.

Chapter 1 References

[1] Shinzo Tamai and Masahiro Kinoshita. Parallel operation of digital controlled ups system. In Industrial Electronics, Control and Instrumentation, 1991. Proceedings. IECON'91., 1991 International Conference on, pages 326–331. IEEE, 1991.

[2] JM Clemmensen. Estimating the cost of power quality. IEEE Spectr, 30(6):40–41, 1993.

[3] Zeng Liu, Jinjun Liu, Xueyu Hou, Qingyun Dou, Danhong Xue, and Teng Liu. Output impedance modeling and stability prediction of three-phase paralleled inverters with master–slave sharing scheme based on terminal characteristics of individual inverters. IEEE Transactions on Power Electronics, 31(7):5306–5320, 2016.

[4] Joachim Holtz, Wolfgang Lotzkat, and K-H Werner. A high-power multitransistor-inverter uninterruptable power supply system. IEEE Transactions on Power Electronics, 3(3):278–285, 1988.

[5] Jiann-Fuh Chen and Ching-Lung Chu. Combination voltage-controlled and current-controlled pwm inverters for ups parallel operation. IEEE Transactions on Power Electronics, 10(5):547–558, 1995.

[6] Prabha Kundur, Neal J Balu, and Mark G Lauby. Power system stability and control, volume 7. McGraw-hill New York, 1994.

[7] Alireza Daneshpooy. Dead-beat control of parallel connected ups. In Applied Power Electronics Conference and Exposition, 2002. APEC 2002. Seventeenth Annual IEEE, volume 1, pages 580–583. IEEE, 2002.

[8] Hiroyuki Hanaoka, Masahiko Nagai, and Minoru Yanagisawa. Development of a novel parallel redundant ups. In Telecommunications Energy Conference, 2003. INTELEC'03. The 25th International, pages 493–498. IEEE, 2003.

[9] Mukul C Chandorkar, Deepakraj M Divan, and Rambabu Adapa. Control of parallel connected inverters in standalone ac supply systems. IEEE Transactions on Industry Applications, 29(1):136–143, 1993.

[10] Josep M Guerrero, José Matas, L Garcia De Vicunagarcia De Vicuna, Miguel Castilla, and Jaume Miret. Wireless-control strategy for parallel operation of distributed-generation inverters. IEEE Transactions on Industrial Electronics, 53(5):1461–1470, 2006.

[11] Josep M Guerrero, L García de Vicuña, Jose Matas, and Jaume Miret. Steady-state invariant-frequency control of parallel redundant uninterruptible power supplies. In IECON 02 [Industrial Electronics Society, IEEE 2002 28th Annual Conference of the], volume 1, pages 274–277. IEEE, 2002.

[12] Jinwei He and Yun Wei Li. Analysis, design, and implementation of virtual impedance for power electronics interfaced distributed generation. IEEE Transactions on Industry Applications, 47(6):2525–2538, 2011.

[13] Hua Han, Xiaochao Hou, Jian Yang, Jifa Wu, Mei Su, and Josep M Guerrero. Review of power sharing control strategies for islanding operation of ac microgrids. IEEE Transactions on Smart Grid, 7(1):200–215, 2016.

[14] Jaehong Kim, Josep M Guerrero, Pedro Rodriguez, Remus Teodorescu, and Kwanghee Nam. Mode adaptive droop control with virtual output impedances for an inverter-based flexible ac microgrid. IEEE Transactions on power electronics, 26(3):689–701, 2011.

[15] Chih-Chiang Hua, Kuo-An Liao, and Jong-Rong Lin. Parallel operation of inverters for distributed photovoltaic power supply system. In Power Electronics Specialists Conference, 2002. pesc 02. 2002 IEEE 33rd Annual, volume 4, pages 1979–1983. IEEE, 2002.

[16] Aris L Dimeas and Nikos D Hatziargyriou. Operation of a multiagent system for microgrid control. IEEE Transactions on Power Systems, 20(3):1447–1455, 2005.

[17] Yajuan Guan, Juan C Vasquez, Josep M Guerrero, and Ernane Antônio Alves Coelho. Small-signal modeling, analysis and testing of parallel three-phase-inverters with a novel autonomous current sharing controller. In 2015 IEEE Applied Power Electronics Conference and Exposition (APEC), pages 571–578. IEEE, 2015.

[18] Jinwei He and Yun Wei Li. An enhanced microgrid load demand sharing strategy. IEEE Transactions on Power Electronics, 27(9):3984–3995, 2012.

[19] Dipankar De and Venkataramanan Ramanarayanan. Decentralized parallel operation of inverters sharing unbalanced and nonlinear loads. IEEE Transactions on Power Electronics, 25(12):3015–3025, 2010.

[20] Anil Tuladhar, Hua Jin, Tom Unger, and Konrad Mauch. Control of parallel inverters in distributed ac power systems with consideration of line impedance effect. IEEE Transactions on Industry Applications, 36(1):131–138, 2000.

2. NESTED CONTROL LOOPS SYSTEM DESIGN FOR GRID-FORMING INVERTERS

2.1. Introduction

The VSIs are the dominant inverters applying to parallel inverters applications. The common switching method, that is PWM, for VSIs and the inverter output LC filter design are concisely presented in this chapter. Besides, since the nested current and voltage control loops system has a considerable effect on power sharing between inverters the design process for this control structure is also discussed in detailed.

In conventional droop control implementation, the VSI is assumed as an ideal voltage source which is connected to the AC bus through an impedance of Z. This impedance basically includes two different components, the inverter output impedance and the impedance of the connecting line. In conventional droop method the impedance Z is considered inductive. As it is mentioned, the control system has a significant effect on inverter output impedance, to showing this fact, it will be proved by Bode plot, that using a control system with inductor current and capacitor voltage feedback provides an almost inductive impedance on the output of the inverter at the fundamental frequency.

2.2. Three-Phase VSIs Topology

Three-phase inverters are usually applied to the high power applications. These inverters can be formed by connecting three single-phase inverters in parallel or using a three-phase bridge [1]. Fig. 2.1 shows the VSI structure in which V_{dc} represents the DC link provided by a DG sources. The switching signals are applied to the switches using PWM technique.

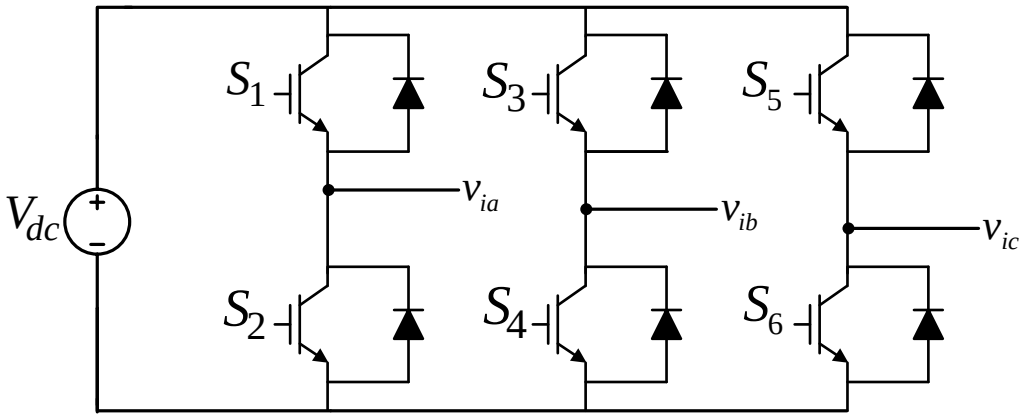

Figure 2.1: Three-phase VSI topology.

2.2.1. Pulse Width Modulation (PWM)

The common approach to provide appropriate control signal for inverter switching is the pulse width modulation (PWM) technique. Two main characteristics for this switching technique are controlling the fundamental frequency and amplitude of the inverter output voltage, and providing the possibility of using a smaller filter to filter the harmonic components out of the output voltage. In order to provide the sinusoidal and balanced three-phase signals at the output of the inverter the switches need to be switched in the specific sequences. Therefore, one sinusoidal reference signal for each of the phases is needed, which is called modulation signal [1]. The output signal frequency is dictated by the reference signal frequency. To form the switching sequence the reference signal is compared with the carrier signal which its frequency dictates the switching frequency. Fig. 2.2 shows the firing pulse generation for S_1 and S_4 using a three-phase PWM, and the $L-L$ voltage (V_{ab}).

The output voltage harmonics appear in the vicinity of the switching frequency and vicinity of its integer coefficients. Since the switching frequency is usually high, the output voltage harmonics are also of the high frequency; therefore, these high frequency harmonics will be simply filtered out using an output filter. Notice that increasing switching frequency shrink the size of the required output filter; nevertheless, increasing switching frequency raises the switching losses.

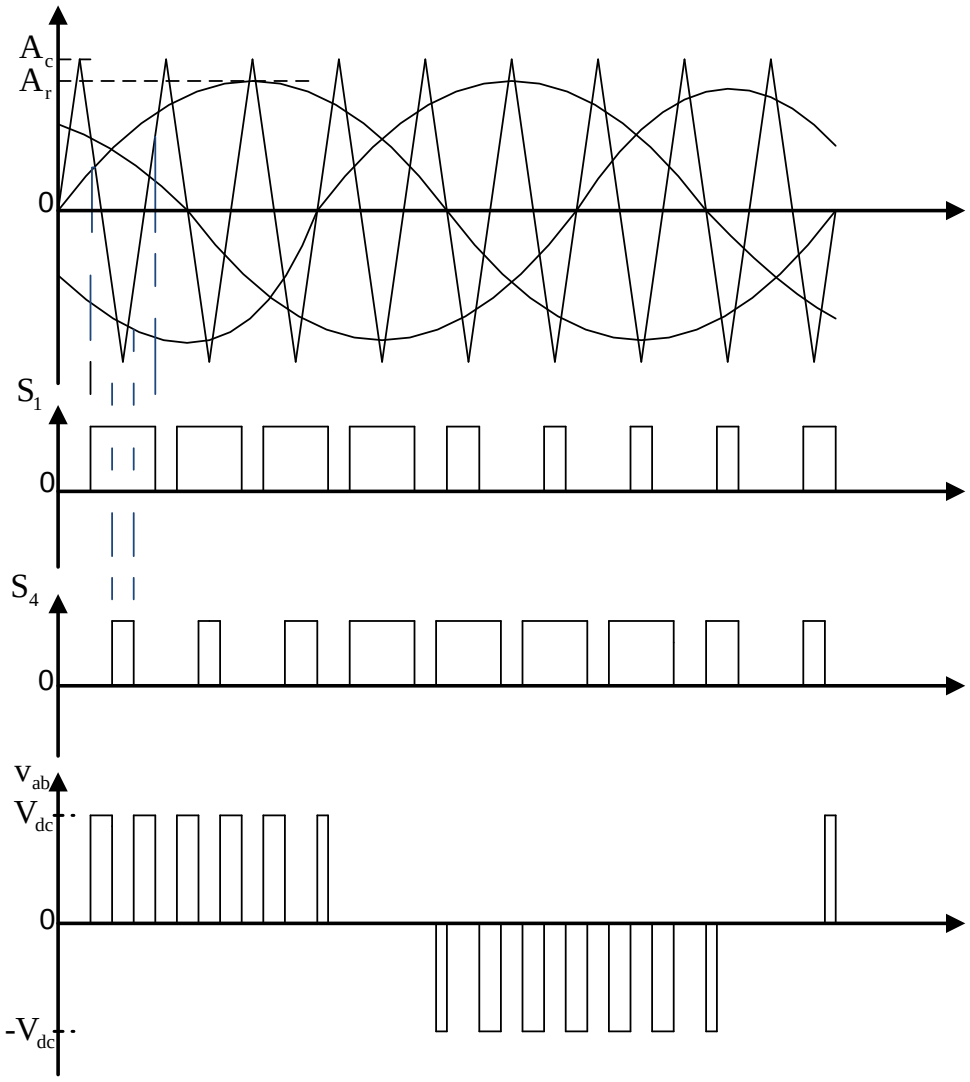

Figure 2.2: Three-phase pwm, firing signals and L-L voltage.

The inverter output voltage amplitude is controlled using the inverter modulation index (m_f), which is defined as the ratio of the amplitude of the reference and carrier signals [2].

$$m_f = \frac{A_r}{A_c} \tag{2.1}$$

$$A_{out} = m_f \times V_{dc} \tag{2.2}$$

Where A_{out} is the inverter output voltage amplitude. As long as the modulation index is less than unit ($m_f < 1$), the amplitude of the output voltage fundamental component is linearly proportional to the modulation index.

2.3. Output Filter Design

The output LC filter is for filtering the undesired harmonic components from the output current and voltage spectrum. From the output filter cost and size effectiveness points of views, it is better to increase the switching frequency, rising the switching frequency, however, raises the switching losses [3]. Therefore, to improving the efficiency a set of limitations need to be considered in output filter design [4, 5].

In order to establish a voltage with low harmonic content, the LC filters are usually used at the output of the inverters. Eq. (2.3) shows the relationship between filter cutoff frequency and its components.

$$f_c = \frac{1}{2\pi\sqrt{L_f C_f}} \tag{2.3}$$

The output voltage harmonic content is the most considerable parameter in output filter design; nevertheless, size, cost, and losses are also effective factors in filter designing process. As an example, if the designer prefers a lower harmonic content at the inverter output, the filter size, cost, and losses will increase or if the designer prefers to minimize the losses then the inverter output harmonic content will increase. It worth to note that a small filter provides a better speed of response and lower output impedance yet a higher harmonic distortion in stable condition.

If the switching frequency is considered as f_{sw}, then by considering the limitations on output current and voltage ripples the filter inductor and capacitor can be selected as follow.

$$L_f = \frac{v_{dc} - V_{out_{rms}}}{2\Delta i_{L_{f_{rms}}} f_{sw}} m_f \tag{2.4}$$

$$C_f = \frac{v_{dc} - V_{out_{rms}}}{16 L_f \Delta v_{C_{f_{rms}}} f_{sw}^2} m_f \tag{2.5}$$

Where $V_{out_{rms}}$ is the rms value of the inverter output voltage. The limitations on the rms value of inductor current ripple ($\Delta i_{L_{f_{rms}}}$) is between %10 to %20 of the rms value of inductor rated current. The rms value of capacitor voltage ripple ($\Delta v_{C_{f_{rms}}}$) is limited to %1 of the rms capacitor voltage [6].

2.4. Nested Voltage and Current Control Loops for Inverter

The three-phase voltage source inverter modeling, as well as, the analysis and design of the control system for a three-phase VSI is presented in this section. The detailed controller design procedure and its effects on the characteristics like bandwidth, system transient and steady state response are explained. Then, the control system effects on the inverter output impedance is discussed.

2.4.1. Modelling of the Three-Phase Voltage Source Inverter

The overall structure of a three-phase voltage source inverter which is followed by an LC filter is depicted in Fig. 2.3. The output of the LC filter is applied to a three-phase load. The governing equation for this system can be simply extracted by considering the average

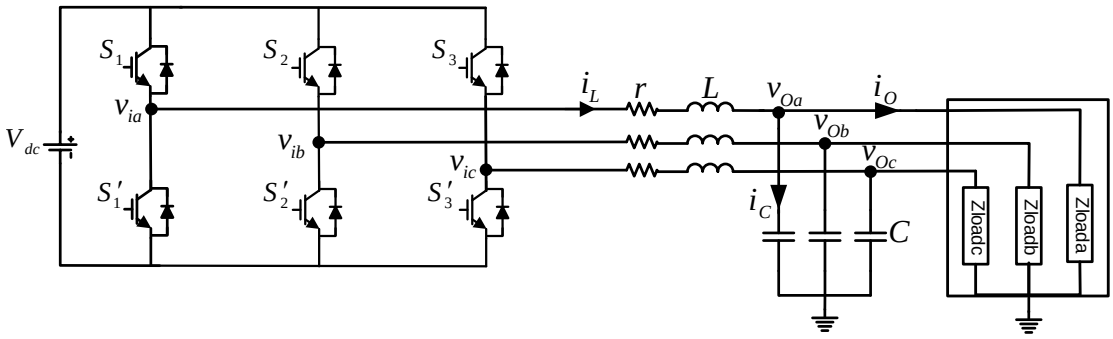

Figure 2.3: The overall structure of the system.

model for the inverter as follow.

$$L\frac{di_{La}}{dt} + ri_{La} = v_{ia} - v_{Oa} \tag{2.6a}$$

$$L\frac{di_{Lb}}{dt} + ri_{Lb} = v_{ib} - v_{Ob} \tag{2.6b}$$

$$L\frac{di_{Lc}}{dt} + ri_{Lc} = v_{ic} - v_{Oc} \tag{2.6c}$$

$$L\frac{dv_{Oa}}{dt} = i_{La} - i_{Oa} \tag{2.7a}$$

$$L\frac{dv_{Ob}}{dt} = i_{Lb} - i_{Ob} \tag{2.7b}$$

$$L\frac{dv_{Oc}}{dt} = i_{Lc} - i_{Oc} \tag{2.7c}$$

Where L and C are the filter inductor and capacitor, r is the equivalent series resistance (ESR) for inductor filter. Using (2.6) and (2.7) the block diagram of the linearized model for each phase of this system is shown in Fig. 2.4.

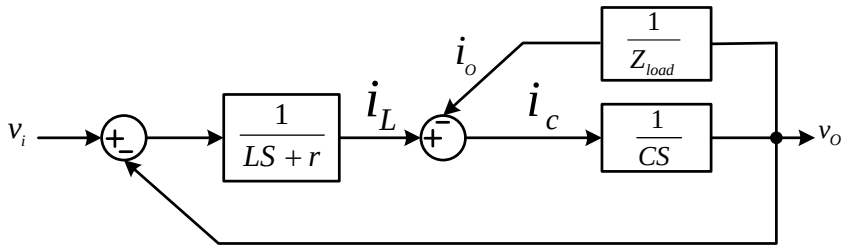

Figure 2.4: Block diagram of linearized model for each phase of the inverter.

2.4.2. Control System Design with the Inductor Current and Capacitor Voltage Feedback Signals

By using the linearized model block diagram of the inverter shown in Fig. 2.4, the current and voltage control loops are designed in this section.

2.4.2.1. Current Control Loop Design

Fig. 2.5 shows the overall structure of the current control loop for each phase of the inverter in which a proportional gain is added to the linearized block diagram of the inverter in Fig. 2.4. Notice that since the output voltage is acting as a disturbance for current control loop a branch of this signal with the opposite sign is added to the current controller to compensate the disturbance effects. Using Fig. 2.5 the current control loop transfer function can simply be extracted as

$$G_i(s) = \frac{i_L}{i_L^*} = \frac{K_{pi}}{Ls + r + K_{pi}} \tag{2.8}$$

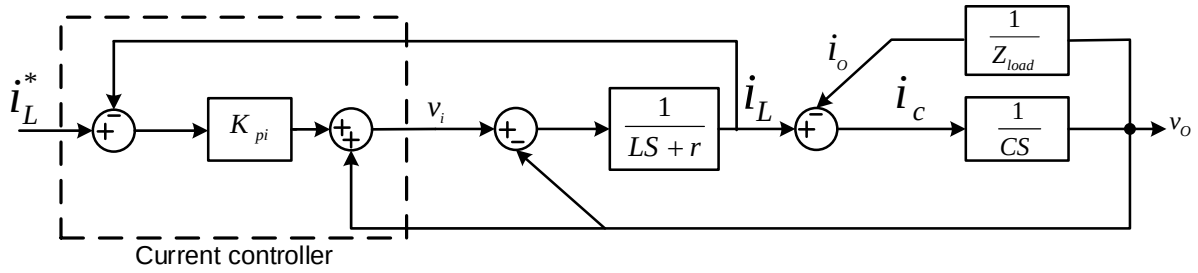

Figure 2.5: Current control loop block diagram.

where i_L^* is the reference for inductor current and K_{pi} is the current proportional controller. In ideal conditions in order to achieve a fast transient response and an acceptable tracking error the current control loop bandwidth needs to be very high [7], which is realizable by choosing a high proportional gain for current controller. High proportional gain, however, results in some issues as:

1. Weakening the system stability in practical implementation
2. Passing the switching noises to the output.

Therefore, the proportional gain is chosen to meet the aforementioned controlling objectives meanwhile to provide an acceptable noise cancellation and appropriate stability to the system. The optimum value for proportional gain needs to be calculated based on the desire bandwidth for current control loop. It is noteworthy that in order to have a acceptable speed of response for current control loop while providing a good disturbance rejection the bandwidth of this loop is usually selected 1/10 of switching frequency [8]. Then, The relation ship between proportional gain and current control loop bandwidth can be derived from (2.8).

$$K_{pi} = r + \sqrt{r^2 + (L \times \omega_{bw})^2} \tag{2.9}$$

where ω_{bw} is the current control loop bandwidth. Table 2.1 summarized the system parameters. Using system parameters and (2.9) the proportional gain is 6.4. The Bode plot for the current control loop transfer function is shown in Fig. 2.6, as it can be seen the current control loop bandwidth is $1000Hz$ which is 1/10 of the switching frequency.

Table 2.1: System parameters.

System Parameters	Rated Value
Inverter rated capacity (KVA)	10
Inductor filter (mH)	1
Inductor ESR (Ω)	0.1
Capacitor filter (μF)	100
DC voltage (V_{dc}) (V)	1200
Switching frequency (KHz)	10
Line-line rms voltage (V)	690

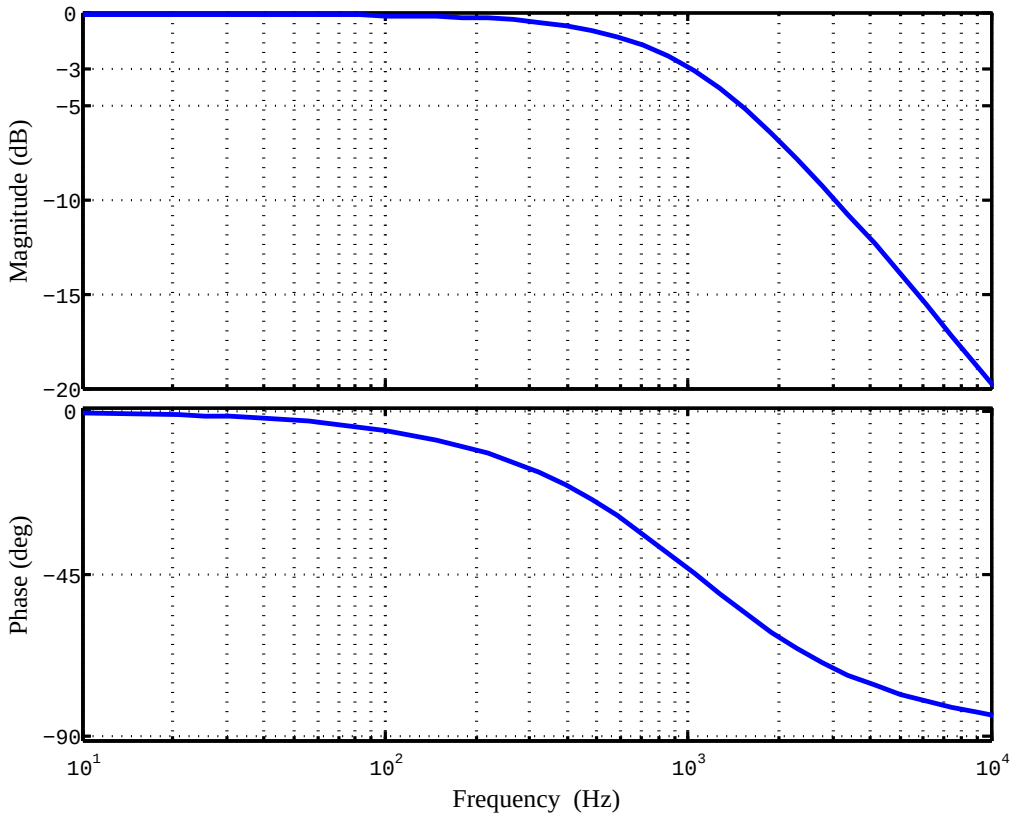

Figure 2.6: Current control loop Bode plot.

Note that at $f_{bw} = \frac{f_{sw}}{10} = 1KHz$, $20log(|G_i(j\omega_{bw})|) = -3dB$; besides, the magnitude of the transfer function at fundamental frequency $(gain(\frac{i_L}{i_L^*})|_{f=60Hz})$ is 0.997 which shows a good reference tracking performance for current control loop.

2.4.2.2. Voltage Control Loop Design

Fig. 2.7 shows the voltage control loop for simplified model of each phase of the inverter. The current control loop is replaced with its equivalent transfer function. As it can be seen the output current acts as disturbance for voltage control loop, this disturbance affects the voltage quality specially when the load changes. Therefore, to compensate the

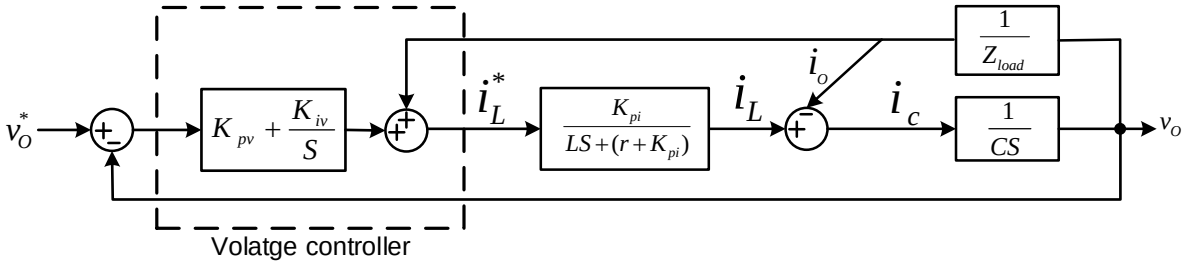

Figure 2.7: Block diagram of voltage control loop for each phase of the inverter.

effects of this disturbance a feedforward branch of the output current with the opposite sign is added to the voltage controller. It is noteworthy that in current control loop effective bandwidth which the current control loop is close to unity the effects of this disturbance is compensated significantly.

A proportional-integrator (PI) controller is served in voltage control loop. Although, the integrator part would cause a phase lag in the output voltage comparing to its reference, achieving an inductive output impedance (which is a basic assumption in implementing the droop control) and a zero tracking error are the advantageous of employing the integrator compensator.

Using Fig. 2.7 the closed-loop transfer function for voltage control loop can simply extracted as (2.10).

$$\begin{aligned} v_o = & \frac{K_{pi}(K_{pv}s + K_{iv})}{LCs^3 + (r + K_{pi})Cs^2 + K_{pv}K_{pi}s + K_{iv}K_{pi}} v_O^* \\ & - \frac{Ls^2 + rs}{LCs^3 + (r + K_{pi})Cs^2 + K_{pv}K_{pi}s + K_{iv}K_{pi}} i_o \triangleq G_v(s)v_O^* - Z_O(s)i_o \end{aligned} \tag{2.10}$$

where K_{pv} and K_{iv} are the proportional and integrator gain for PI controller, respectively. $G_v(s) = \frac{v_O}{v_O^*}$ and $Z_O(s) = \frac{v_O}{i_O}$ are called the voltage control and output impedance transfer functions, respectively. Fig. 2.8 and Fig. 2.9 show the Bode plot for $G_v(s)$ and $Z_O(s)$, respectively. The designed parameters for PI controller are $K_{pv} = 4$, $K_{iv} = 820$, as it can be seen in Fig. 2.8 using the system parameters the voltage transfer function gain at fundamental frequency ($60Hz$) is almost unity with zero phase shift. Besides, the high bandwidth of this transfer function will assure an appropriate transient response for the system.

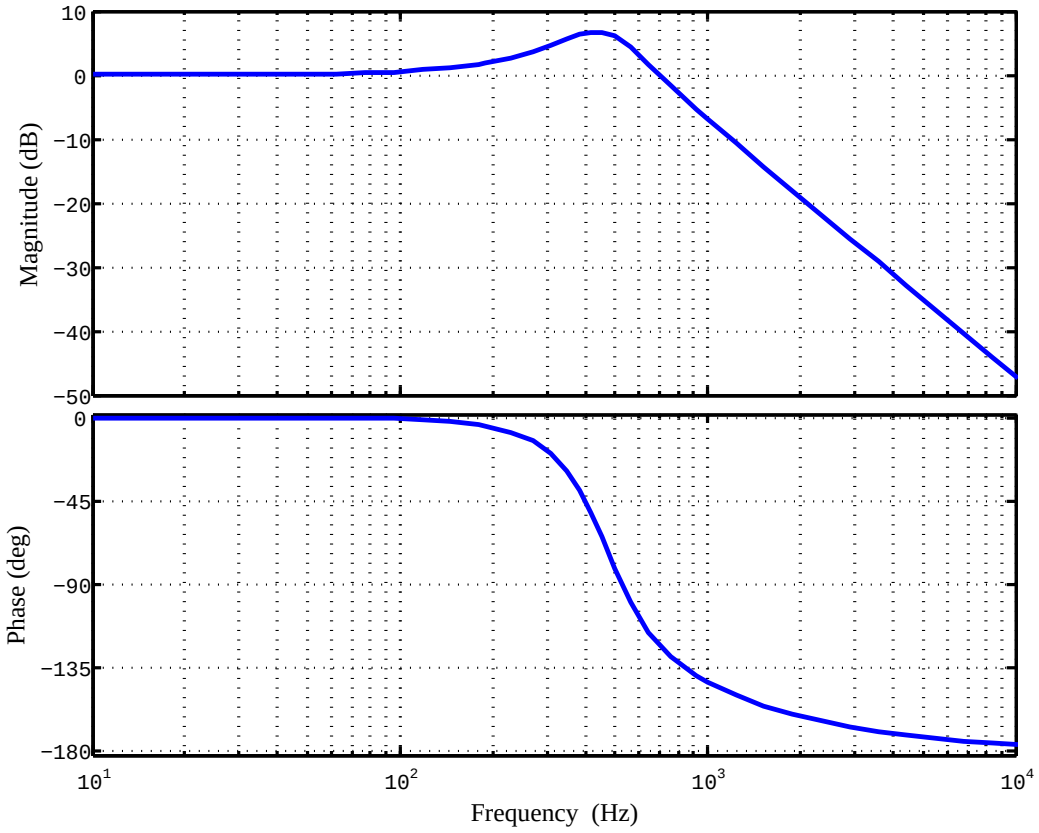

Figure 2.8: Bode plot for voltage control transfer function.

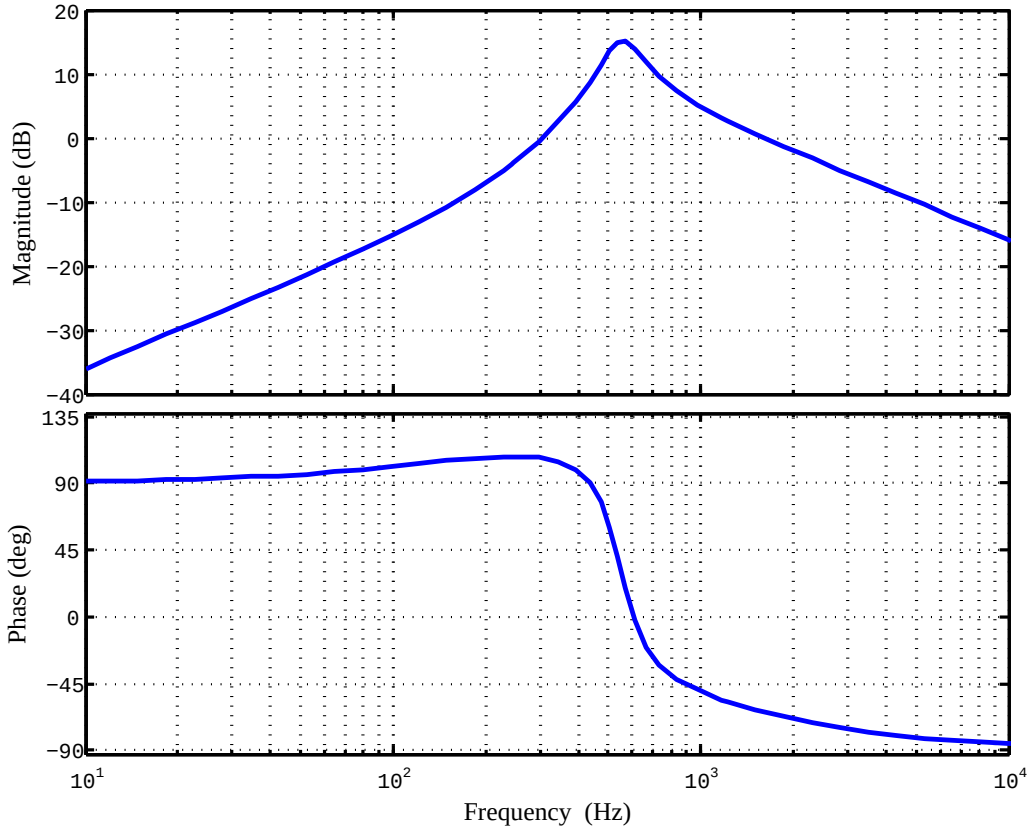

Figure 2.9: Inverter output impedance Bode plot.

As it can be seen in Fig. 2.9 the inverter output impedance shows an almost inductive characteristic at fundamental frequency, which is an appropriate impedance for power control of the inverter using the droop control method.

2.5. Simulation Results

In order to verify the control system performance, the simulation results for this control system are provided. The simulation is conducted under linear and nonlinear loads to evaluate the performance and transient response of the designed control system. Fig. 2.10 and Fig. 2.11 show the simulation results for three-phase inverter output voltage and current when the inverter is supplying an RL load ($R = 10\Omega$, $L = 0.25mH$).

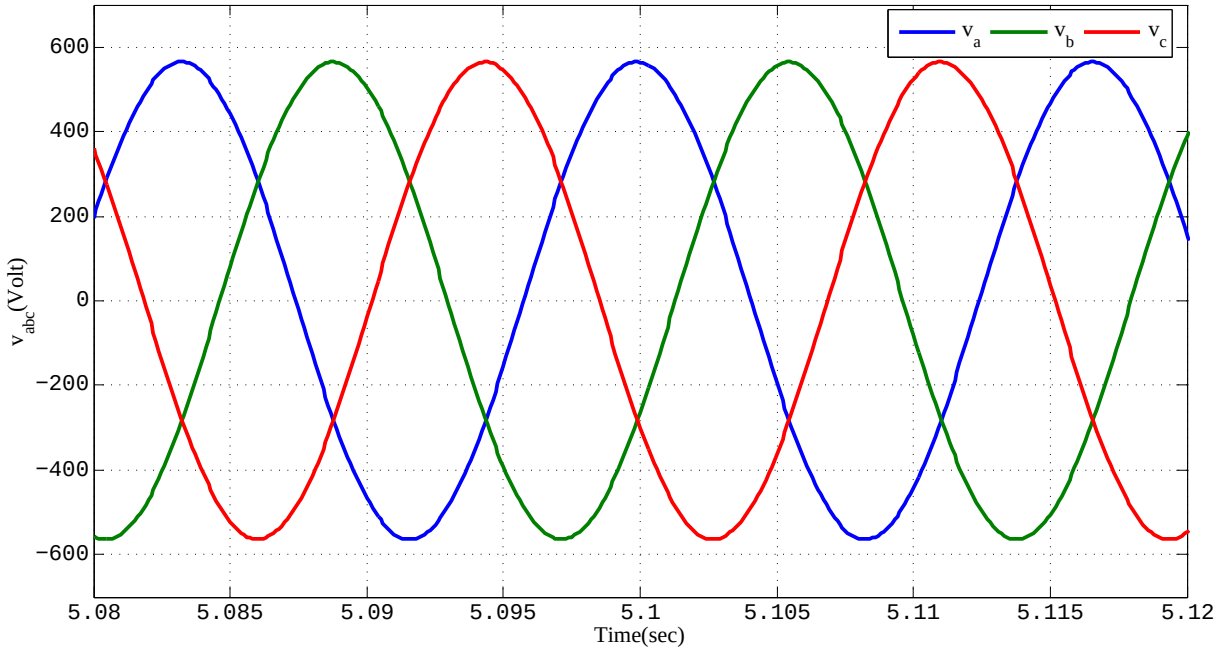

Figure 2.10: Inverter output three-phase voltage.

Fig. 2.12 and Fig. 2.13 show the three-phase inverter output voltage and current in load changing conditions. As it can be seen the transition response of the control system is fast and stable.

Fig. 2.14 shows the output current for phase A of the inverter when the inverter is supplying a nonlinear load. The nonlinear load is a three-phase rectifier which followed by a capacitor of $C = 1200\mu F$ and is loaded with a resistive load of $R = 55\Omega$.

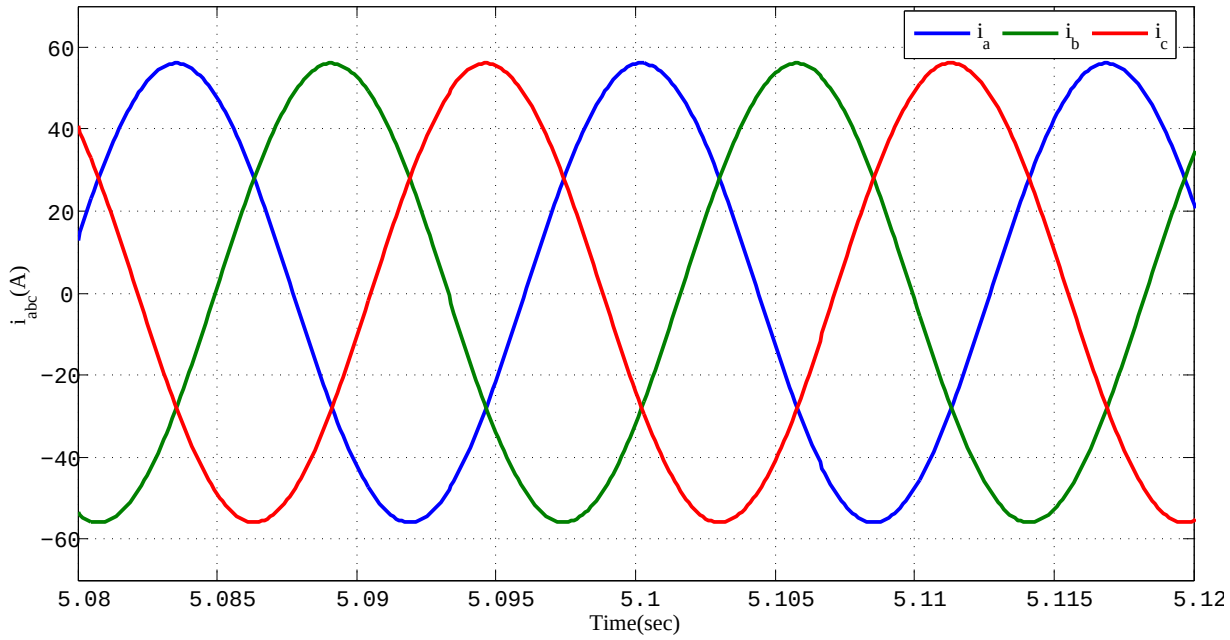

Figure 2.11: Inverter output three-phase current.

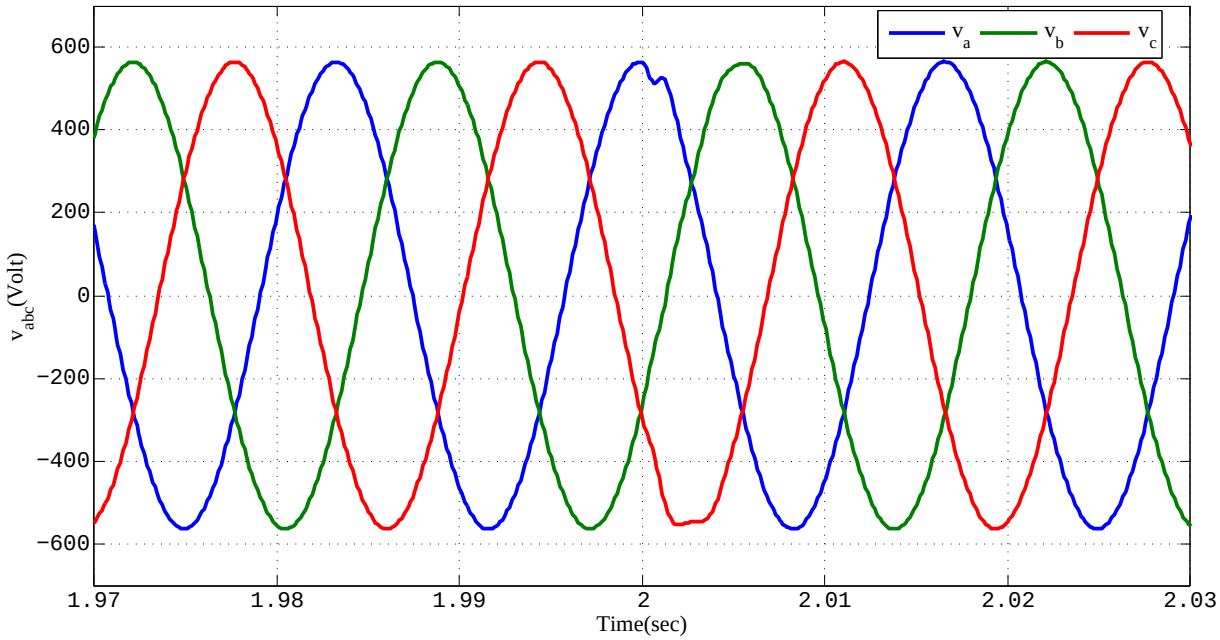

Figure 2.12: Output voltage transition response.

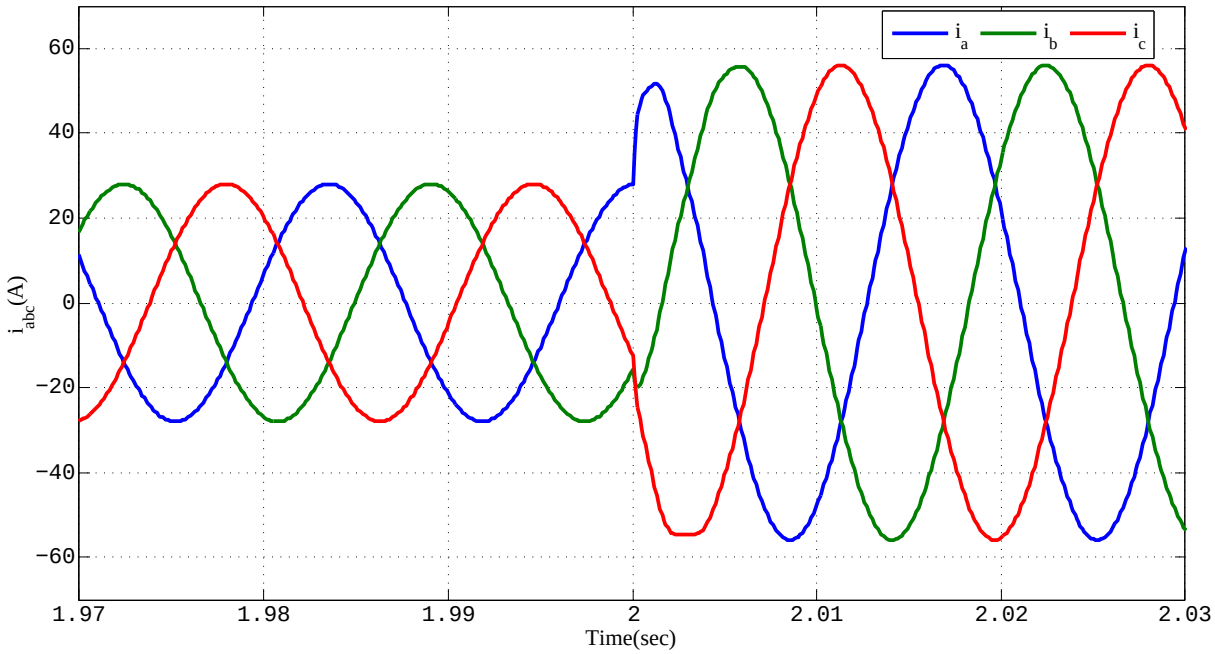

Figure 2.13: Output current transition response.

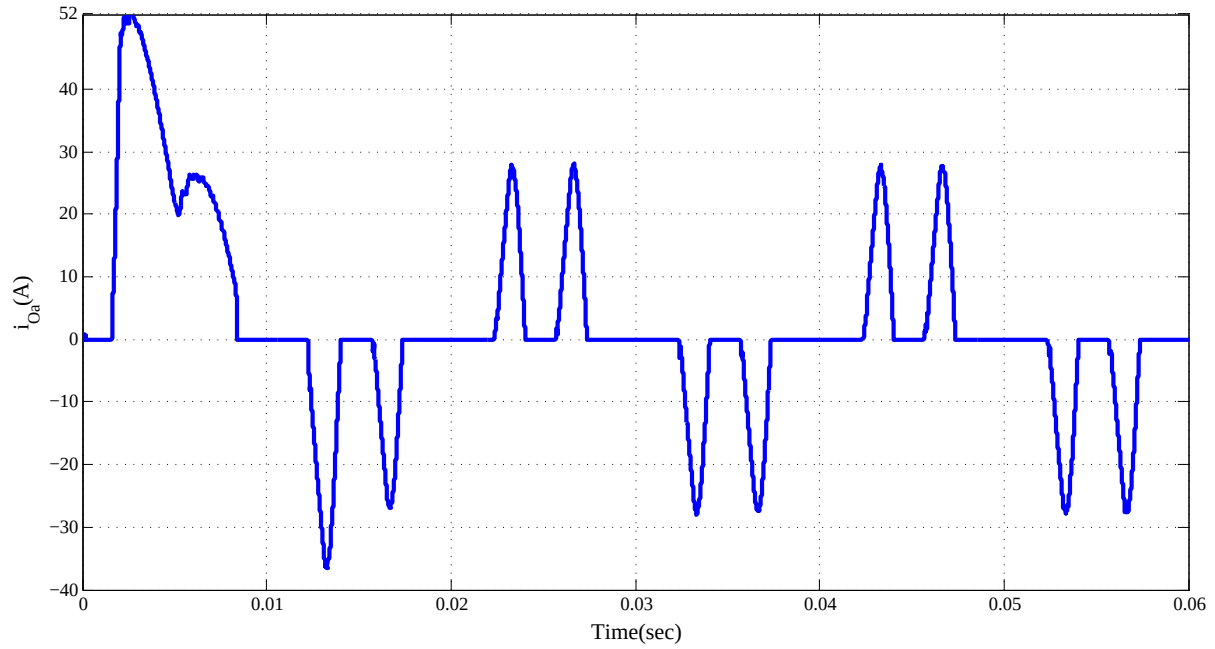

Figure 2.14: Nonlinear output current for phase A of the inverter.

Chapter 2 References

[1] Muhammad Harunur Rashid. Power electronics: devices, circuits, and applications. PEARSON, 2014.

[2] Muhammad H Rashid. Power electronics handbook: devices, circuits and applications. Academic press, 2010.

[3] Milan Prodanovic and Timothy C Green. Control and filter design of three-phase inverters for high power quality grid connection. IEEE transactions on Power Electronics, 18(1):373–380, 2003.

[4] Khaled H Ahmed, Stephen J Finney, and Barry W Williams. Passive filter design for three-phase inverter interfacing in distributed generation. In 2007 Compatibility in Power Electronics, pages 1–9. IEEE, 2007.

[5] Timothy CY Wang, Zhihong Ye, Gautam Sinha, and Xiaoming Yuan. Output filter design for a grid-interconnected three-phase inverter. In Power Electronics Specialist Conference, volume 2, pages 779–784. IEEE 34th Annual, 2003.

[6] Little Box Challenge. Detailed inverter specifications, testing procedure, and technical approach and testing application requirements for the little box challenge. ht tps://www. littleboxchallenge. com/pdf/LBC-InverterRequirements-20141216. pdf [Online: accessed 18-JAN-2015], 2015.

[7] Mohammad Monfared, Saeed Golestan, and Josep M Guerrero. Analysis, design, and experimental verification of a synchronous reference frame voltage control for single-phase inverters. IEEE transactions on Industrial Electronics, 61(1):258–269, January 2014.

[8] Sushil S Thale, Rupesh G Wandhare, and Vivek Agarwal. A novel reconfigurable microgrid architecture with renewable energy sources and storage. IEEE transactions on Industrial Applications, 51(2):1805–1816, April 2015.

3. DIRECT CURRENT VECTOR CONTROL (DCVC) FOR GRID-FOLLOWING INVERTERS

3.1. Introduction

Depending on conditions and applications the inverter-interfaced DG sources may operate in grid-connected or islanded mode. In grid-connected mode the inverters are usually controlled in current control mode. One of the developed current control techniques is the direct current control method (DCVC), which directly controls the inverter output current within the converter physical constraints. However, this control technique is in voltage-oriented rotating reference frame (VORRF) which is also called synchronous reference frame (SRF). In this chapter the SRF is briefly presented first, and then the DCVC method is investigated in details.

3.2. Synchronous Reference Frame (SRF)

One of the issues associated with stationary reference frames (abc and $\alpha\beta$) is the steady state reference tracking error when the PI controllers are employed to control the signals. To overcome this issue while still using the PI controllers the sinusoidal signals can be transferred to DC signals using synchronous reference frame transformations. Fig. 3.1 shows this transformation graphically, as it can be seen the three-phase balanced sinusoidal signals (a, b, and c) are transformed to two rotating DC signals (d and q) with the angular velocity of ω. The SRF transformation is realizable using the transformation matrix, T_{abc-dq}.

$$T_{abc-dq} = \frac{2}{3}\begin{bmatrix} \cos(\theta) & \cos\left(\theta - \frac{2\pi}{3}\right) & \cos\left(\theta - \frac{4\pi}{3}\right) \\ -\sin(\theta) & -\sin\left(\theta - \frac{2\pi}{3}\right) & -\sin\left(\theta - \frac{4\pi}{3}\right) \end{bmatrix}$$

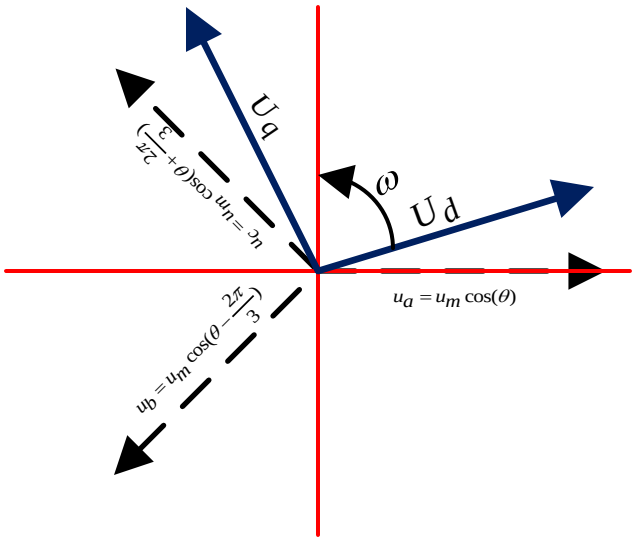

Figure 3.1: Voltage-oriented rotating reference frame.

where $\theta = \int \omega dt$, and the DC-rotating signals, which are called d and q, can be calculated as follow.

$$\begin{bmatrix} U_d \\ U_q \end{bmatrix} = T_{abc-dq} \cdot \begin{bmatrix} u_a \\ u_b \\ u_c \end{bmatrix} \tag{3.1}$$

It is worth noting that if the rms value of abc signals is defined as U, then by considering a balanced three-phase system $U_d = U$ and $U_q = 0$ [1, 2].

3.3. Modeling Voltage Source Inverter (VSI) in SRF

Fig. 3.2 shows a grid-connected VSI, which is connected to the grid through and LC filter. By considering the average model for the converter and applying the KVL and KCL rules, the dynamic governing equation for this converter can be derived as

$$v_{i\_abc} = R_f i_{L_{f-abc}} + L_f \frac{di_{L_{f-abc}}}{dt} + v_{C_{f-abc}} \tag{3.2}$$

$$i_{L_{f-abc}} = C_f \frac{dv_{C_{f-abc}}}{dt} + i_{o\_abc}. \tag{3.3}$$

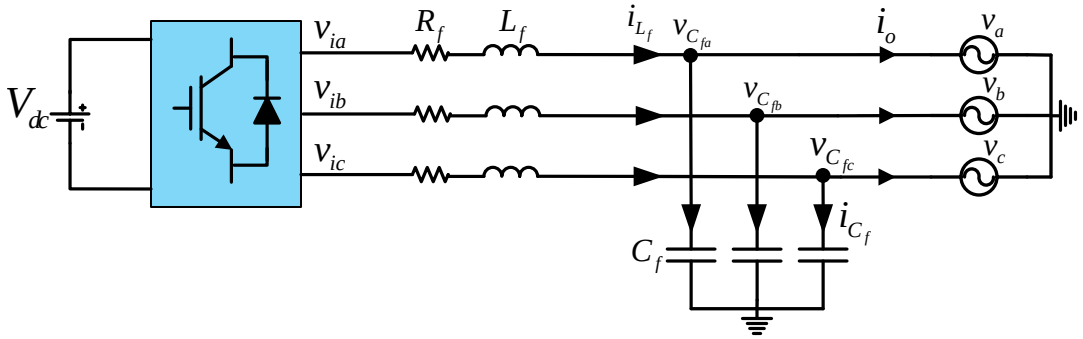

Figure 3.2: Grid-connected inverter.

If we define the matrix which transforms the dq signals back to abc signals as T_{dq-abc}, then we can reorganize the Eq. (3.2) as Eq. (3.4).

$$T_{dq-abc} = \begin{bmatrix} \cos(\theta) & -\sin(\theta) \\ \cos\left(\theta - \frac{2\pi}{3}\right) & -\sin\left(\theta - \frac{2\pi}{3}\right) \\ \cos\left(\theta - \frac{4\pi}{3}\right) & -\sin\left(\theta - \frac{4\pi}{3}\right) \end{bmatrix}$$

$$[T_{dq-abc}] \begin{bmatrix} v_{id} \\ v_{iq} \end{bmatrix} - [T_{dq-abc}] \begin{bmatrix} v_{Cd} \\ v_{Cq} \end{bmatrix} = \tag{3.4}$$
$$R_f [T_{dq-abc}] \begin{bmatrix} i_{Ld} \\ i_{Lq} \end{bmatrix} + L_f \frac{d}{dt}([T_{dq-abc}]) \begin{bmatrix} i_{Ld} \\ i_{Lq} \end{bmatrix} + L_f [T_{dq-abc}] \frac{d}{dt} \begin{bmatrix} i_{Ld} \\ i_{Lq} \end{bmatrix}.$$

Where v_{id} and v_{iq} are the inverter output voltage d and q components, v_{Cd} and v_{Cq} are the filter capacitor voltage in synchronous reference frame, and i_{Ld} and i_{Lq} are the d and q components of the filter inductor current . By considering

$$[T_{abc-dq}][T_{dq-abc}] = \begin{bmatrix} 1 & 0 \\ 0 & 1 \end{bmatrix}, [T_{abc-dq}] \cdot \frac{d}{dt}[T_{dq-abc}] = \omega \cdot \begin{bmatrix} 0 & -1 \\ 1 & 0 \end{bmatrix}$$

and multiplying $[T_{abc-dq}]$ by (3.4) then the Eq. (3.4) can be redefined as

$$\begin{bmatrix} v_{id} \\ v_{iq} \end{bmatrix} = R_f \begin{bmatrix} i_{Ld} \\ i_{Lq} \end{bmatrix} + L_f \frac{d}{dt} \begin{bmatrix} i_{Ld} \\ i_{Lq} \end{bmatrix} + L_f \omega \begin{bmatrix} -i_{Lq} \\ i_{Ld} \end{bmatrix} + \begin{bmatrix} v_{Cd} \\ v_{Cq} \end{bmatrix}. \tag{3.5}$$

Applying the same procedure to Eq. (3.3) results in

$$C_f \frac{d}{dt} \begin{bmatrix} v_{Cd} \\ v_{Cq} \end{bmatrix} + C_f \omega \begin{bmatrix} -v_{Cq} \\ v_{Cd} \end{bmatrix} = \begin{bmatrix} i_{Ld} \\ i_{Lq} \end{bmatrix} - \begin{bmatrix} i_{od} \\ i_{oq} \end{bmatrix}. \tag{3.6}$$

In steady state the derivative terms in (3.5) and (3.6) are zero; therefore, these two equation stes can be represented as (3.7) and (3.8).

$$v_{idq} = R_f i_{Ldq} + j L_f \omega i_{Ldq} + v_{Cdq} \tag{3.7}$$

$$j C_f \omega v_{Cdq} = i_{Ldq} - i_{odq} \tag{3.8}$$

where v_{idq}, i_{Ldq}, v_{Cdq} and i_{odq} stand for the steady-state space vectors of inverter output voltage, LC-filter inductor current, capacitor filter voltage, and grid current in voltage oriented dq reference frame.

3.4. Direct Current Vector Control Implementation

3.4.1. Inner Control Loop

The equations (3.7) and (3.8) are the base principles for implementing the direct-current control of the grid connected inverter. In DCVC technique the main concept lays on the directly control of the output current sending from converter to the grid and the controller tries to dictate the output current as the controlling signal. therefore, by considering the dq output current as controlling signals ($i_d^{'}$ and $i_q^{'}$) Eq. (3.8) will change to

$$j C_f \omega v_{Cdq} = i_{Ldq} - i_{odq}^{'}. \tag{3.9}$$

Substituting (3.9) in (3.7) results in (3.10) and (3.11).

$$v_{id} = R_f i_d^{'} - L_f \omega i_q^{'} + (1 - L_f C_f \omega^2) v_{Cd} - (R_f C_f \omega) v_{Cq} \tag{3.10}$$

$$v_{iq} = R_f i_q^{'} + L_f \omega i_d^{'} + (R_f C_f \omega) v_{Cd} + (1 - L_f C_f \omega^2) v_{Cq} \tag{3.11}$$

Using (3.10) and (3.11) the block diagram for inner current control loop of the DCVC technique can be developed as Fig. 3.3, where $R_{eq} = R_f$, $L_{eq} = L_f$, $v_{Cd}^{'} = (1 - L_f C_f \omega^2) v_{Cd} - R_f C_f \omega v_{Cq}$, and $v_{Cq}^{'} = R_f C_f \omega v_{Cd} + (1 - L_f C_f \omega^2) v_{Cq}$. It is noteworthy that the output of

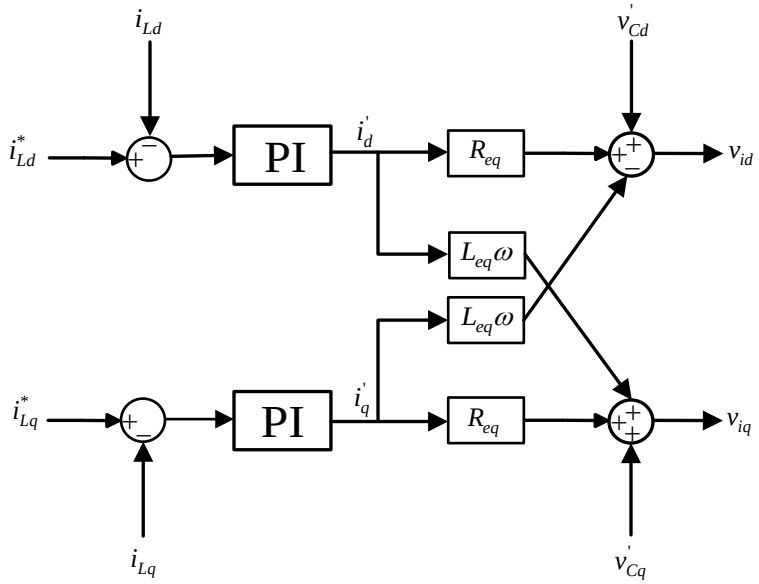

Figure 3.3: Current control loop for DCVC technique.

the current control loops are the dq current signals. These current signals are used as tuning currents and the controller input error signals would guide the controllers to adjust the tuning currents during dynamic control process [3].

3.4.2. Outer Control Loop

The instantaneous active and reactive powers delivered to the point of common coupling (PCC), the bus at which the converter is coupled to the grid, can be calculated in

synchronous reference frame as follow.

$$p(t) = v_d i_d + v_q i_q \tag{3.12}$$

$$q(t) = v_q i_d - v_d i_q \tag{3.13}$$

However, these powers contains harmonics; therefore, active and reactive powers first are filtered through low-pass filters and then applied to the power control loop which is the outer control loop. Usually, in order to coordinate the power control loops with inner control loops the low-pass filter cutoff frequency is chosen very low to have make the outer control loops slow enough while filtering all the harmonics out of the powers. Fig. 3.4 shows the outer power control loops which are added to the DCVC block diagram. Where P^* and Q^* are

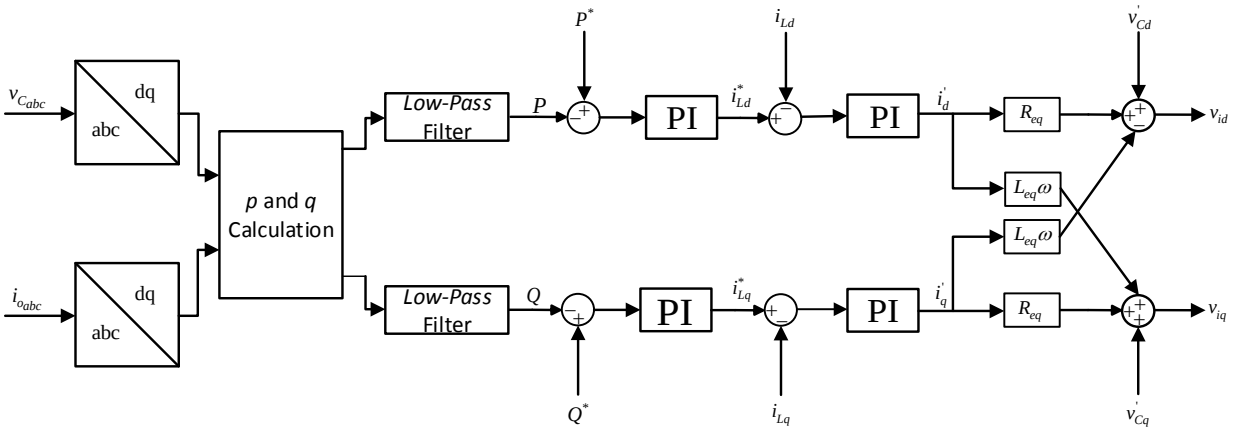

Figure 3.4: Integrating the outer control loop in DCVC block diagram.

the references for active and reactive powers, respectively. It is noteworthy that the outer control loop can be dc-link voltage and bus-voltage controller, instead of active and reactive power control.

3.4.3. Control Under Converters Physical Constraints

In practice, the voltage source converter (VSC) should operate under rated power and PWM saturation limits. To satisfy such conditions, the design strategy of the DCVC [4, 5] is to control the VSC by maintaining the effectiveness of the PCC active power control as

the first priority while meeting the PCC reactive power control demand as much as possible when the VSC reaches its rated power or PWM saturation limit. This is expressed as:

Minimize: $|q - q^*|$

Subject to: $p = p^*$, $\sqrt{i_{Ld}^2 + i_{Lq}^2} \leq I_{rated}$, $\sqrt{\frac{v_{id}^2 + v_{iq}^2}{3}} \leq \frac{V_{dc}}{2\sqrt{2}}$

The requirement is implemented in the following way. To prevent the converter from exceeding the rated current, (3.14) is employed if the amplitude of the reference current generated by the outer control loop exceeds the rated current limit. According to (3.7) and (3.8), this represents a strategy of keeping the d-axis current reference i_{Ld}^* unchanged so as to maintain active power or dc-link voltage control effectiveness while modifying the q-axis current reference i_{Lq}^* to satisfy the reactive power or ac system bus voltage control demand as much as possible [5]. If $|v_{idq}|$ generated by the current control loops exceeds the PWM saturation limit, v_{id}^* and v_{iq}^* are modified by (3.14).

$$i_{Ld-new}^* = i_{Ld}^*, i_{Lq-new}^* = sign(i_{Lq}^*).\sqrt{(i_{Ldq-max}^*)^2 - (i_{Ld}^*)^2} \tag{3.14}$$

Therefore, the current and voltage limiters should be integrated in the nested-control loops system, and the control system will be improved as follow.

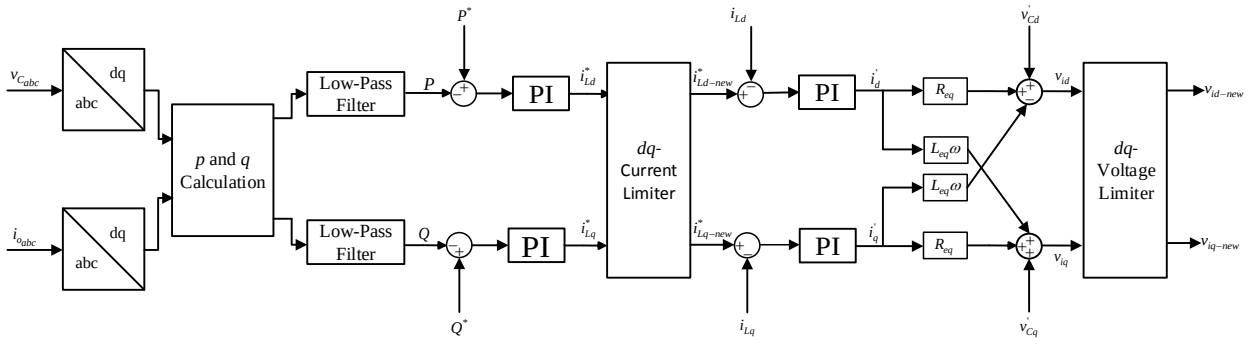

Figure 3.5: Applying converter physical constraints to DCVC.

3.5. Simulation Results

To evaluate the nested-control loops system performance, especially the current control loop, and the system transient response the simulation is conducted under different load

scenario. Table 3.1 shows the system parameters, which also includes the control system parameters. The inverter-interfaced DG system is connected to the grid at $t = 1.5s$. Then

Table 3.1: System parameters.

System Parameters	Value
Inverter rated capacity (KVA)	80
Inductor filter (mH)	1
Inductor ESR (Ω)	0.1
Capacitor filter (μF)	100
DC voltage (V_{dc}) (V)	1200
Switching frequency (KHz)	6
Line-line rms voltage (V)	690
d-axis current controller proportional gain	0.08
d-axis current controller integral gain	105
q-axis current controller proportional gain	0.08
d-axis current controller integral gain	105
Bus-voltage controller proportional gain	1.36
Bus-voltage controller integral gain	44.49
RL load	(20+j4)Ω
Resistive load	30 kW

a heavy resistive load is added to the RL load at $t = 6s$, the resistive load is disconnected at $t = 10s$. Fig. 3.6 and 3.7 show the three-phase current and voltage transition responses when the second load is added to the system.

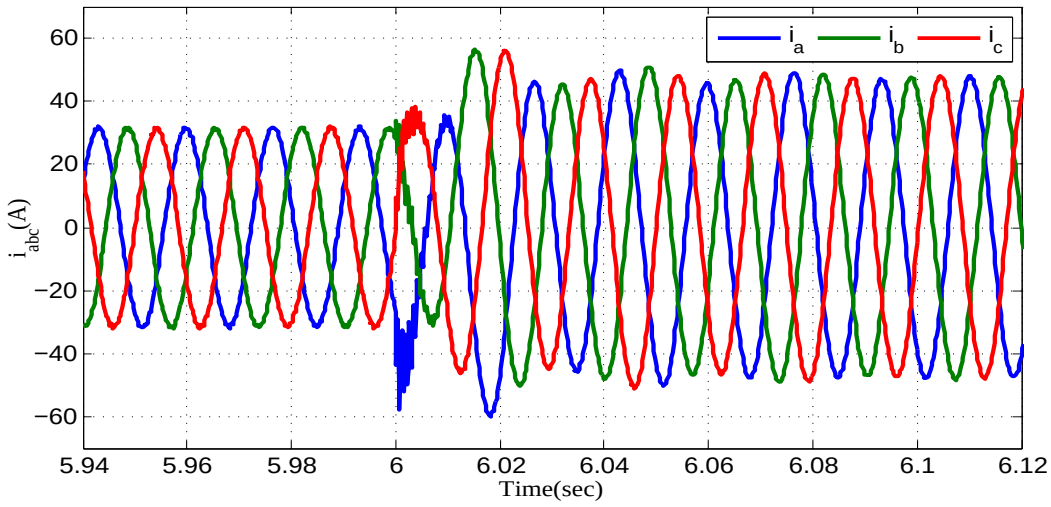

Figure 3.6: Inverter output three-phase transition current.

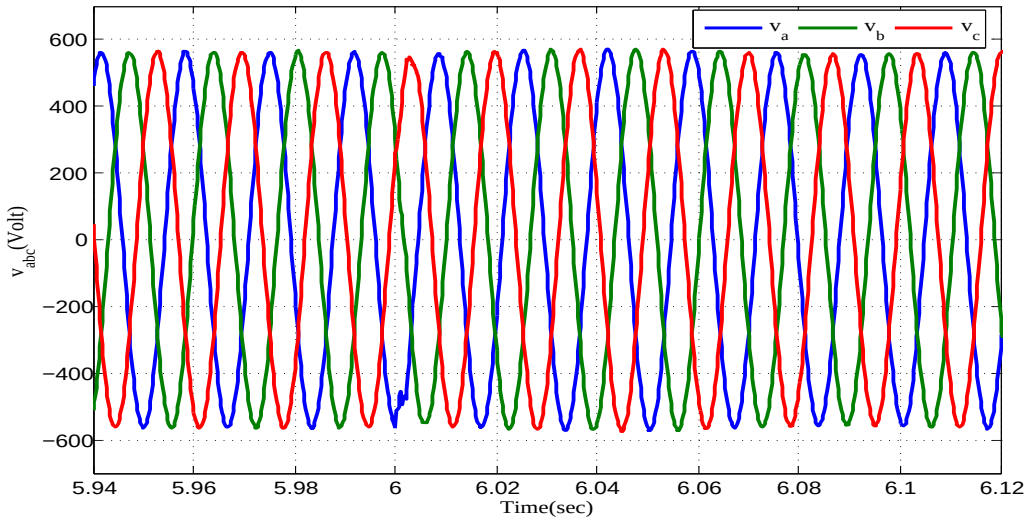

Figure 3.7: Inverter output three-phase voltage at transition time.

It is necessary to mention that in simulation the outer-control loop includes the bus-voltage controller and the d-axis current reference is changed based on the load demand to evaluate the controller performance.

Fig. 3.8 and 3.9 shows the d and q current reference tracking for current control loop during different transients in load changing. As it can be seen in Fig. 3.8 by changing the d-axis current at different times the output d-axis current tracks the reference very fast with zero steady state error. By changing the load at different times the reactive power and

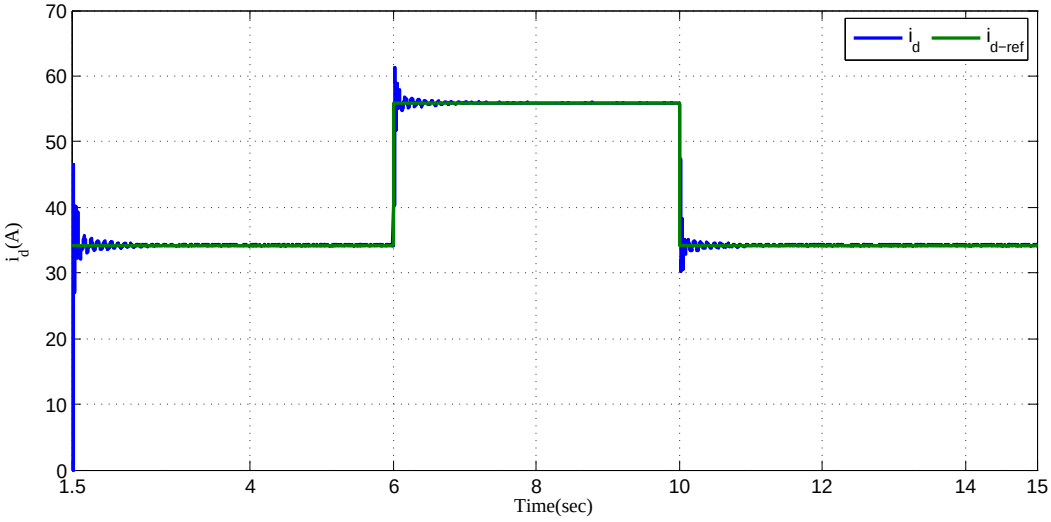

Figure 3.8: D-axis current reference tracking.

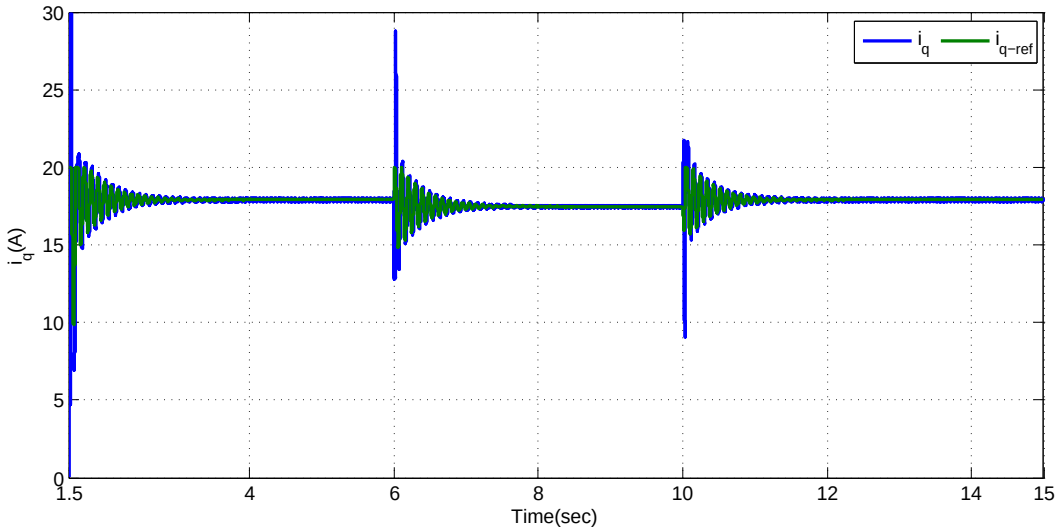

Figure 3.9: Q-axis current reference tracking.

consequently the bus voltage changes; therefore, the q-axis current reference changes. This variation is obvious from Fig. 3.9 and as it can be seen the q-axis current tracks its reference quickly with zero steady state error.

Fig. 4.15 shows the inverter output active and reactive power changing during different load scenarios.

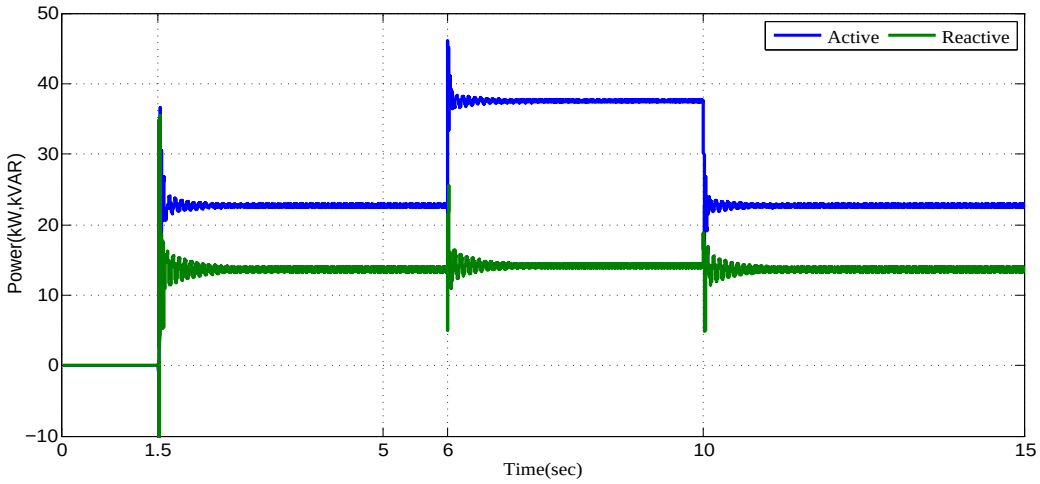

Figure 3.10: Inverter output active and reactive powers.

Chapter 3 References

[1] Nagaraju Pogaku, Milan Prodanovic, and Timothy C Green. Modeling, analysis and testing of autonomous operation of an inverter-based microgrid. IEEE Transactions on power electronics, 22(2):613–625, 2007.

[2] Lennart Harnefors. Modeling of three-phase dynamic systems using complex transfer functions and transfer matrices. IEEE Transactions on Industrial Electronics, 54(4):2239–2248, 2007.

[3] Simon Haykin and Neural Network. A comprehensive foundation. Neural Networks, 2(2004), 2004.

[4] Shuhui Li, Timothy A Haskew, and Ling Xu. Control of hvdc light system using conventional and direct current vector control approaches. IEEE Transactions on Power Electronics, 25(12):3106–3118, 2010.

[5] Shuhui Li, Timothy A Haskew, Yang-Ki Hong, and Ling Xu. Direct-current vector control of three-phase grid-connected rectifier–inverter. Electric Power Systems Research, 81(2):357–366, 2011.

4. POWER CONTROL SYSTEM DESIGN FOR PARALLEL INVERTERS

4.1. Introduction

In the islanding operation of distributed *ac* power supply systems, distributed generation (DG) units are usually connected through inverters to an ac distribution system. Different methods have been developed to control the parallel inverters or more specifically the power sharing among different DGs. One of the common methods for controlling inverters in the islanding mode is the droop method, which has an advantage of being a wireless control method [1]. This is an important benefit for the droop control method especially when different DGs are located far from each other and there is no possibility of building a communication link between these units [2]. One of the issues associated with conventional droop control method to control the parallel inverters is the reactive power sharing while supporting the bus voltage, which results in bus voltage drop [3].

In this chapter the power control system is designed based on the droop control method; besides, by integrating the DCVC method with droop method the bus voltage drop issue inherent in conventional droop method is solved. One of the inverter-interfaced distributed generation (DG) systems is considered as the grid-forming unit and the other one which is a DCVC-Droop control system based unit is connecting to the PCC to support the *ac* bus. The power control system for DCVC-Droop system is based on the integrating the droop-based power control loop with DCVC-based current control loop to supply the demanded active power and support the reactive power within the converter physical constraints.

4.2. Power Flow Analysis of a Single Unit

To power sharing analysis, the power flow of a single inverter-interfaced DG needs to be investigated, firstly. Fig. 4.1 shows a single DG source which is connected through an inverter and transmission line to the *ac* bus.

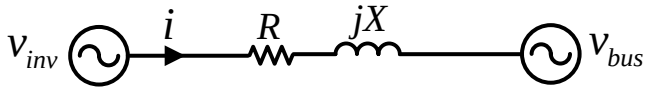

Figure 4.1: Single inverter-interfaced DG connected to *ac* bus.

Considering the phasor equivalent for inverter output voltage and bus voltage as

$$v_{inv} = V_1 \angle \delta_1, v_{bus} = V^{'} \angle \delta^{'}$$

, and the transmission line as

$$z_t = |Z| \angle \theta.$$

Where

$$|Z| = \sqrt{R^2 + X^2}, \theta = \tan^{-1}\left(\frac{X}{R}\right).$$

Then, the apparent power flow from DG source to the PCC can be presented as follow [4]

$$S = V_1 e^{j\delta_1} I^* \tag{4.1}$$

where S is called the apparent power and I^* is the complex conjugate for the phasor form of the current i in Fig. 4.1.

$$I = \frac{V_1 e^{j\delta_1} - V^{'} e^{j\delta^{'}}}{|Z| e^{j\theta}} \tag{4.2}$$

Therefore, by mathematic manipulation the apparent power is as

$$S = p + jq = \frac{V_1^2 - V_1 V^{'} cos(\delta_1 - \delta^{'})}{\sqrt{R^2 + X^2}}.cos(\theta) + \frac{V_1 V^{'} sin(\delta_1 - \delta^{'})}{\sqrt{R^2 + X^2}}.sin(\theta) \\ + j\frac{V_1^2 - V_1 V^{'} cos(\delta_1 - \delta^{'})}{\sqrt{R^2 + X^2}}.sin(\theta) - \frac{V_1 V^{'} sin(\delta)}{\sqrt{R^2 + X^2}}.cos(\theta) \tag{4.3}$$

If we assume that the transmission line is dominantly inductive, meaning $\theta = \frac{\pi}{2}$, and define the power angle as $\delta = \delta_1 - \delta^{'}$, then

$$p = \frac{V_1 V^{'}}{X} sin(\delta) \tag{4.4}$$

$$q = \frac{V_1(V_1 - V^{'} cos(\delta))}{X}. \tag{4.5}$$

As it can be concluded from (4.4) and (4.5) when the power angle is very small

$$p = \frac{V_1 V^{'}}{X}(\delta) \tag{4.6}$$

$$q = \frac{V_1(V_1 - V^{'})}{X}. \tag{4.7}$$

meaning that the active power mainly depends on the power angle and reactive power mainly depends on the voltage amplitude difference between DG and *ac* bus. Therefore, active and reactive power can be controlled using conventional droop control method, and the droop characteristics are as follow [5].

$$\omega_1 = \omega_0 - m_1 P \tag{4.8}$$

$$V_1 = V_0 - n_1 Q \tag{4.9}$$

Where ω_0 and V_0 are the references for angular frequency and voltage amplitude, respectively, m_1 and n_1 are called droop coefficients. P and Q are the average value of active and reactive powers, respectively. Fig.4.2 shows the droop power control implementation for an inverter.

It is worth noting that in Fig. 4.2 low-pass filters are employed to calculate the average value of active and reactive powers.

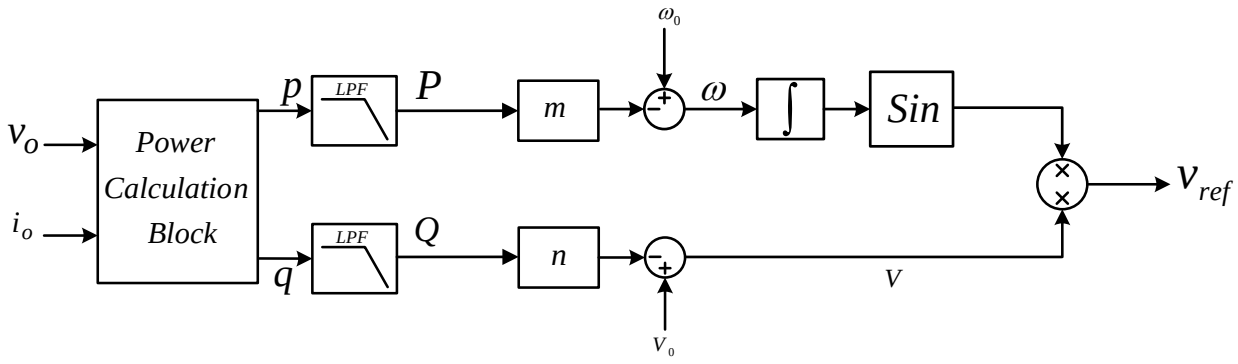

Figure 4.2: Droop power control block diagram.

4.3. Parallel Connected Inverters

4.3.1. Applying Droop Control Method to Parallel Inverters

In distributed *ac* power supply systems the DG sources, which may be located at the different locations of the system, are connected to a point of common coupling (PCC) through connecting lines. In droop-based power control of these parallel inverter-interfaced DGs, when the load changes the units will react to the load changing by dropping in their frequency and voltage amplitude until they finally settle in an identical frequency and voltage amplitude in lower level and share the load according to their capacity [6].

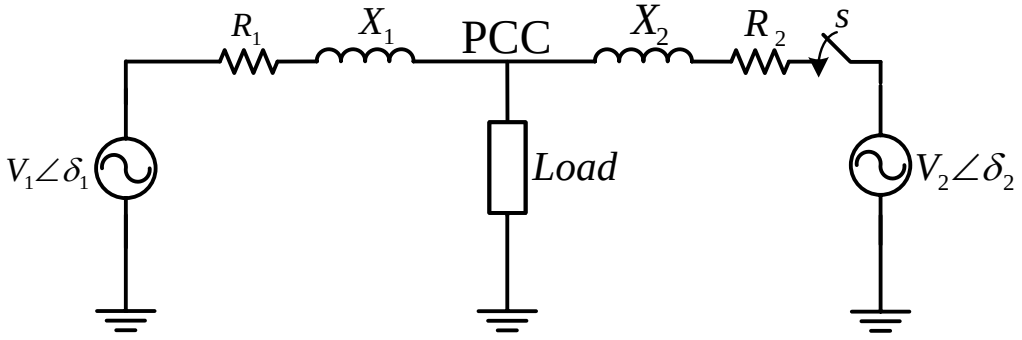

Figure 4.3: Two parallel inverter-interfaced DGs connected to the PCC.

Fig. 4.3 shows two units connected to the PCC through different transmission lines and supplying the loads at the PCC. It is noteworthy that the first unit is the grid forming

unit and after stabilizing the *ac* bus voltage the switch s will be closed and the second unit will also participate in load sharing and supporting the bus voltage.

To investigate the power sharing between two parallel inverters based on the droop method assume two units are connected to the PCC and are in the steady state condition. The active power-frequency droop relationships for these two units are as follow

$$\omega_1 = \omega_0 - m_1 P_1 \tag{4.10}$$

$$\omega_2 = \omega_0 - m_2 P_2 \tag{4.11}$$

then subtracting (4.11) from (4.10) results in

$$\omega_1 - \omega_2 = (m_2 P_2 - m_1 P_1). \tag{4.12}$$

As it is mentioned before, in steady state condition two units reach to an identical frequency, and (4.12) will result in

$$m_1 P_1 = m_2 P_2 \tag{4.13}$$

It needs to be mentioned that droop coefficient will be selected according to the units capacity; therefore, if two units have the same capacity, then $m_1 = m_2 = m$, or as an example if the second unit capacity is twice of the first unit then $m_2 = \frac{m_1}{2}$.
If the number of units will be added then

$$m_1 P_1 = m_2 P_2 = ... = m_i P_i \tag{4.14}$$

where i is the number of the units. Fig. 4.4 shows the active power sharing for two parallel inverters with different capacity, as it can be seen at the steady state the angular frequency for both units is identical and the units share the active power according to their capacity. In this case it is assumed that the first unit has a higher capacity.

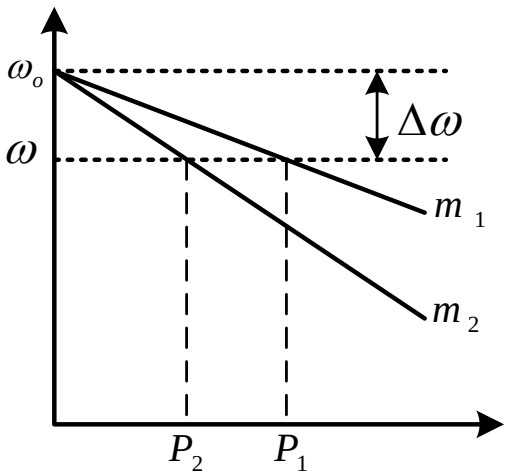

Figure 4.4: Active power sharing between parallel inverters based on their droop characteristics.

Similarly in the case when transmission lines are equal for voltage droop relating to reactive power sharing the droop characteristics are as follow.

$$V_1 = V_0 - n_1 Q_1 \tag{4.15}$$

$$V_2 = V_0 - n_2 Q_2 \tag{4.16}$$

then subtracting (4.16) from (4.16) results in

$$V_1 - V_2 = (n_2 Q_2 - n_1 Q_1). \tag{4.17}$$

In steady state condition $V_1 = V_2 = V$; therefore,

$$n_1 Q_1 = n_2 Q_2 \tag{4.18}$$

and for i units connected to the PCC

$$n_1 Q_1 = n_2 Q_2 = ...n_i Q_i \tag{4.19}$$

The reactive power sharing between two units based on the units droop characteristic is shown in Fig. 4.5.

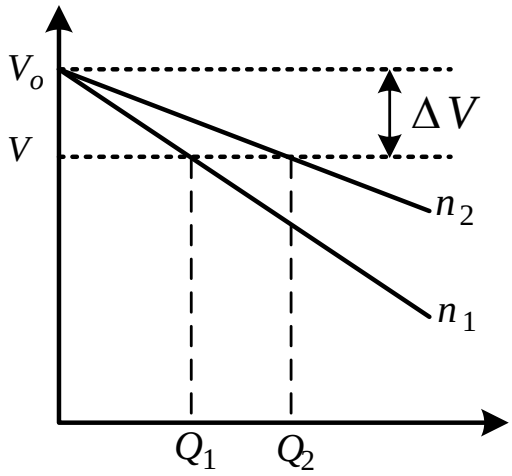

Figure 4.5: Reactive power sharing between two parallel inverters based on their droop characteristics.

However, in real conditions the DG units are located at the different distances from PCC and the transmission lines may not be equal. Therefore, when the transmission lines are not equal $V_1 \neq V_2$ and the reactive power will not be shared appropriately.

In addition, when the reactive power control is based on the conventional droop method,

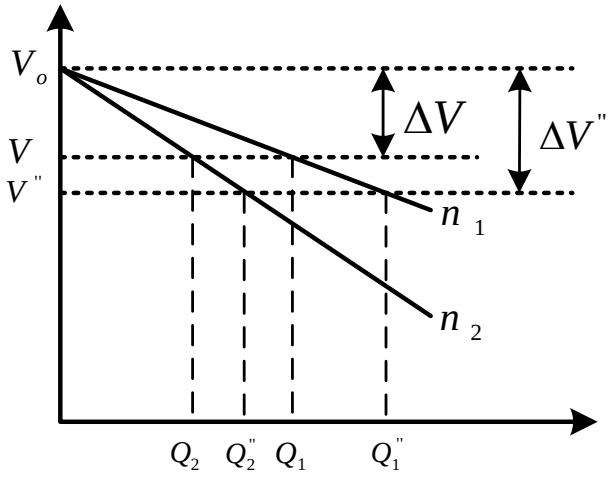

Figure 4.6: Voltage drop associated with reactive power sharing between parallel inverters based on conventional droop method.

increasing in reactive load will be responded by more drop in voltage amplitude as it is shown

in Fig. 4.6, which is not desired from bus voltage deviation limit point of view. Therefore, to deal with aforementioned issues, the integrating of DCVC and conventional droop control methods is proposed in this research.

4.3.2. Integrating Droop and DCVC

Integrating the DCVC control method with droop control method will help to share the active power between parallel inverters based on their rated capabilities and control the bus voltage by injecting enough reactive power to the PCC within converters physical constraints. The active power control in this method is based on the conventional droop control; however, implementing the bus voltage controller helps to control bus voltage and share the reactive power as much as possible.

In Droop-DCVC nested control loops system the droop based active power control and bus voltage control are employed as outer control loop; besides, the inner control loop is a direct current control based loop. The power reference generated by the droop control mechanism is passed to the active power and PCC bus voltage control loop. At this loop, the DCVC control strategy is operated by maintaining the effectiveness of the PCC active power control as the first priority while meeting the PCC bus voltage control demand as much as possible. Therefore, the reactive generation of the converter is determined by the PCC bus voltage controller with the consideration of the physical constraints of the converter, which overcomes the challenge of achieving reactive power droop control among parallel inverters and helps to improve the bus voltage [7].

Fig. 4.7 shows the integration of conventional active power droop control in DCVC system. As it can be seen from Fig. 4.7 the frequency variation resultant from load changing is used through droop characteristic to calculate (as (4.20)) the load required power and this power is used as the reference active power for the unit. The output power of the inverter will be calculated and then compare to reference to generate the reference d-axis current, and the bus voltage controller generates the reference q-axis current.

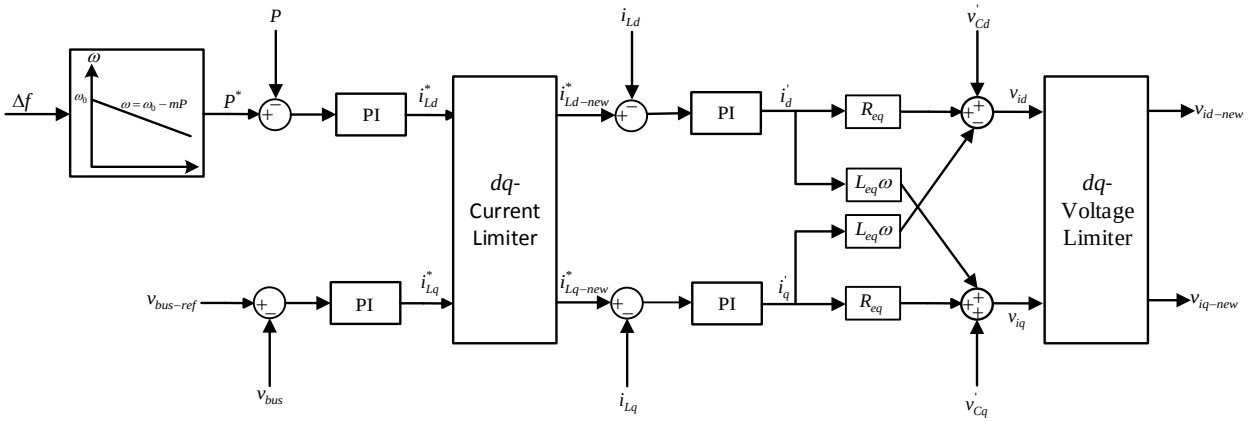

Figure 4.7: Integration active power droop control in DCVC system.

$$P^* = \frac{\Delta\omega}{m} \tag{4.20}$$

Where $\Delta\omega = 2\pi\Delta f$, and Δf is measured using a synchronous reference frame phase-locked loop (PLL).

4.3.3. Applying DCVC and Droop Control to Parallel Inverters

In islanding mode, when parallel DG units are disconnected from the grid, it is necessary to establish the common bus voltage and simultaneously providing the demanded active and reactive powers. Based on this strategy, a DG unit should attempt to balance the power demand while regulating the voltage and stabilizing the frequency of the autonomous microgrid.

A grid-forming unit within a microgrid is assigned to regulate the voltage at the PCC, dominantly set the system frequency, and provide a reference to other vector controlled inverters. The unit should be adequately large and have adequate reserve capacity to supply the power balance. Its function is similar to a traditional slack bus generator and is a necessary component for operation of other vector controlled inverters.

Conventionally, frequency-droop and voltage-droop control strategies without using vector control mechanism were used to share real and reactive powers among two or more DG units. However, this would cause a challenge of reactive power sharing and a bad power

quality to the distributed *ac* system as well [7].

With DCVC, it is possible to integrate vector control and droop control together for control of parallel inverters with improved power quality and reliability. However, DCVC requires that at least one inverter or DG unit within the microgrid must operate as a grid forming unit. Fig. 4.8 shows DCVC and droop control applied to two parallel inverters. The upper

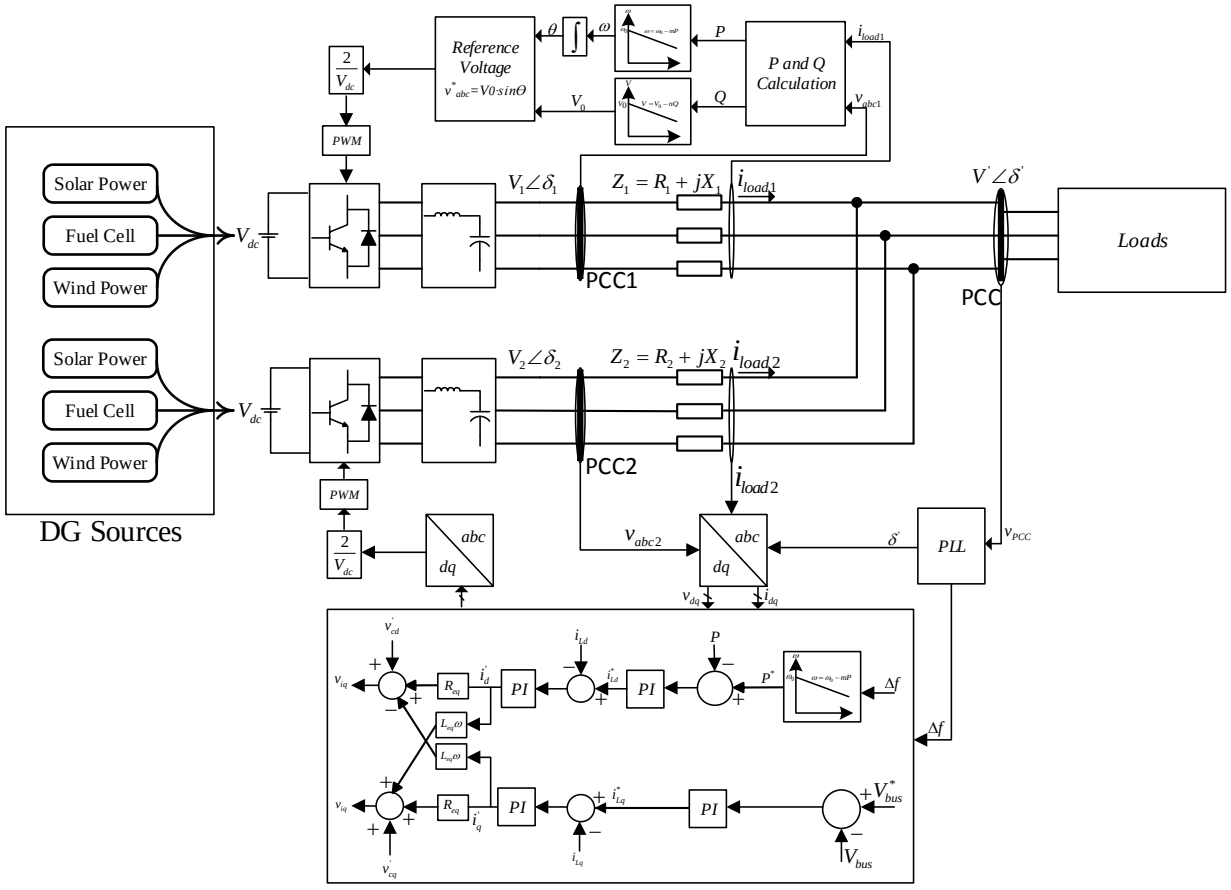

Figure 4.8: Overall structure for DCVC and droop controlled parallel units in islanded mode [7].

part of Fig. 4.8 shows the grid-forming inverter and the control structure. The active and reactive powers are calculated based on the measured output voltage and current at the PCC, and then are used to generate frequency and amplitude signals for control of the grid-forming converter through the conventional droop method. The frequency and amplitude from the active and reactive power droop controllers together formulate the three-phase reference control voltage which is used to drive the PWM to control the converter.

4.3.4. Secondary-Level Power Control

Distributed *ac* power supply systems are forming the microgrids. Microgrid control is typically classified into a three-level hierarchical control involving primary, secondary, and tertiary control, where primary and secondary levels are related to the operation of a microgrid itself, and tertiary level takes care of the coordinated operation of networked microgrids.

Secondary control is the highest hierarchical level when a microgrid is operated in an islanded mode and is responsible for the reliable, secure and economical operation of the microgrid. Secondary control issues control commands to the primary controllers of the DERs within a microgrid and operates on a slower time frame as compared to the primary control. The purposes of this time frame difference include (i) decoupling secondary control from primary control, (ii) reducing the communication bandwidth between the secondary control system and the primary controllers, and (iii) allowing enough time to perform complex calculations such as finding an optimal or most economic way to maintain microgrid frequency stability [8]. It needs to be mentioned that the references for the secondary control level are commanded from microgrid control center (MGCC).

The integration of the primary and secondary control mathematically is achieved by modifying (4.8) as

$$\omega_i = \omega_{0i} - m_i \left(P_i - P_i^*\right) \tag{4.21}$$

where P_i^* is the reference active power from the secondary control for the i^{th} unit. According to (4.21), if the actual active power production of a distributed energy resource (DER), P_i, equals the reference active power from the secondary control, P_i^*, the inverter will maintain the desired frequency for the PCC bus voltage. If P_i is higher than P_i^* due to the load increase, the microgrid frequency will drop, and the secondary control needs to increase reference power commands, P_i^*, in order to boost the frequency to the reference values. If P_i is smaller than P_i^* due to the load decrease, the microgrid frequency will go up, and the secondary control needs to reduce reference power commands, P_i^*, in order to bring the

frequency back to the reference value. Before receiving an updated power reference, the power balance is handling through the primary control mechanism though.

The reactive power control and bus voltage control is handles by bus voltage control loop as it is mentioned in Section 4.3.2. Fig. 4.9 shows the integration of DCVC with droop (Droop-DCVC) and secondary control, in which the droop controller generates an incremental active power reference in real time according to the frequency deviation of the microgrid, the active power reference from the secondary control is updated in $10s$ second scale, the addition of the two together formulates the final active power reference to the DCVC controller, and the PCC bus voltage is controlled directly through the DCVC controller.

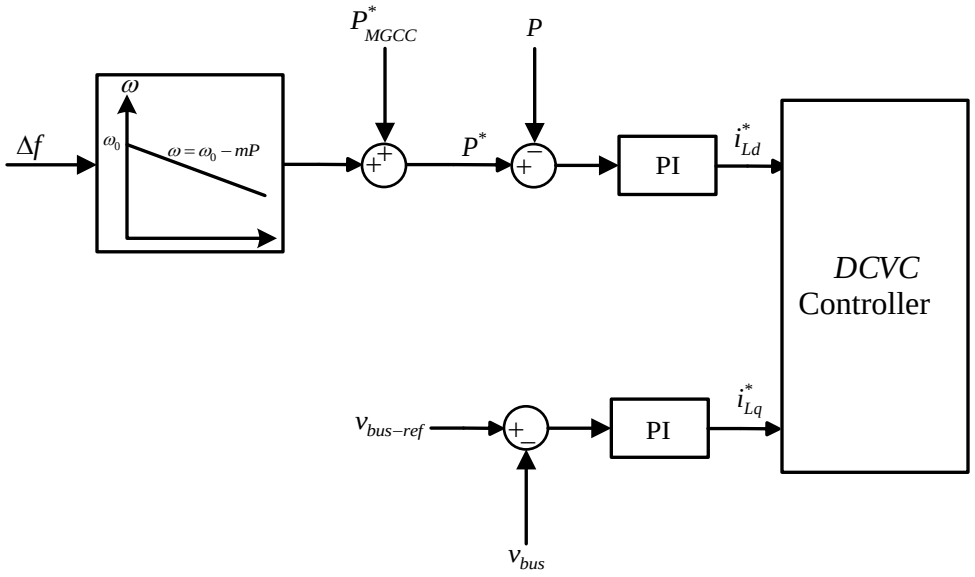

Figure 4.9: Integration of secondary control with power controller.

4.4. Dynamic Response

In implementing the droop method the average value of active and reactive powers are applied to droop characteristics. To calculating the average value of these powers, low-pass filters with high time-constant are usually employed, as it is shown in Fig. 4.2. The high time constant will assure the achieving of an appropriate filtering; however, the low cut-off frequency of these low-pass filters causes a slow dynamic response. To improve the dynamic

response the droop coefficients need to be chosen as high as possible, by considering the system stability and drop limitations on frequency and voltage of the system [9].

In order to design the droop coefficients the droop characteristic equations in (4.8) and (4.9); besides, the power flow equations in (4.4) and (4.5) are considered in the vicinity of an operating point, say $(V_e, V_e^{'}, \delta_e)$. Then by modeling the low-pass filters as the first-order transfer functions, the power flow equations (4.4) and (4.5) will be linearized as follow.

$$\Delta P = \frac{\omega_c}{s+\omega_c}\left(\frac{\partial p}{\partial V}\Delta V + \frac{\partial p}{\partial \delta}\Delta\delta\right) \tag{4.22}$$

$$\Delta Q = \frac{\omega_c}{s+\omega_c}\left(\frac{\partial q}{\partial V}\Delta V + \frac{\partial q}{\partial \delta}\Delta\delta\right) \tag{4.23}$$

where

$$\frac{\partial p}{\partial V} = \frac{V_e^{'}}{X}\sin\delta_e$$

$$\frac{\partial p}{\partial \delta} = \frac{V_e V_e^{'}}{X}\cos\delta_e$$

$$\frac{\partial q}{\partial V} = \frac{2V_e}{X} - \frac{V_e}{X}\cos\delta_e$$

$$\frac{\partial q}{\partial \delta} = \frac{V_e V_e^{'}}{X}\sin\delta_e$$

and Δ implies a small deviation from operation point, and ω_c is the low-pass filters cut-off frequency.

Linearizing (4.8) and (4.9) results in

$$\Delta\omega = -m\Delta P \tag{4.24}$$

$$\Delta V = -n\Delta Q. \tag{4.25}$$

Substituting (4.22) and (4.23) in (4.24) and (4.25) and replacing $\Delta\omega$ with $s\Delta\delta$ gives the following relationships for power angle and voltage amplitude dynamic variations.

$$s\Delta\delta = -m\frac{\omega_c}{s+\omega_c}\left(\frac{\partial p}{\partial V}\Delta V + \frac{\partial p}{\partial \delta}\Delta\delta\right) \tag{4.26}$$

$$\Delta V = -n\frac{\omega_c}{s+\omega_c}\left(\frac{\partial q}{\partial V}\Delta V + \frac{\partial q}{\partial \delta}\Delta\delta\right). \tag{4.27}$$

rearranging (4.27) to evaluate ΔV and substituting the resultant ΔV in (4.26) results in the 3rd order homogenous differential equation for power angle as follow.

$$\left[s^3 + K_1 s^2 + K_2 s + K_3\right]\Delta\delta = 0 \tag{4.28}$$

where

$$K_1 = \omega_c\left[2 + n\frac{\partial q}{\partial V}\right]$$

$$K_2 = \omega_c\left[n\omega_c\frac{\partial q}{\partial V} + m\frac{\partial p}{\partial \delta}\right]$$

$$K_3 = \omega_c^2\left[m\frac{\partial p}{\partial \delta} + mn\left(\frac{\partial p}{\partial \delta}\frac{\partial q}{\partial V} - \frac{\partial p}{\partial V}\frac{\partial q}{\partial \delta}\right)\right].$$

Notice that the system stability analysis and the droop coefficients design for a desired dynamic response are simply possible, by inspecting the poles location for (4.28).

Fig. 4.10 shows the system poles location for different values of frequency droop coefficient ($0 < m < 1 \times 10^{-4}$). The arrows direction shows the poles location change by changing m. AS it can be seen by increasing the droop coefficient one of the three real poles scats from imaginary axis and the two others become the complex-conjugate poles and the dominant poles. The dominant poles dictate the system stability and dynamic response. Although, the complex-conjugate poles are getting closer to the imaginary axis and make the dynamic response to be faster, these poles increase the fluctuation in the system response

and weaken the system dynamic stability. Therefore, the dynamic response of the system is a trade off between speed of the response and the dynamic stability. Note that in Fig. 4.10 the equilibrium operation point is $(V_e, V_e^{'}, \delta_e)$, where $V_e = \left(\sqrt{2} \times \frac{690}{\sqrt{3}}\right) Vrms$, $V_e^{'} = 0.98 \times V_e$, and $\delta_e = 0.0174 rad$.

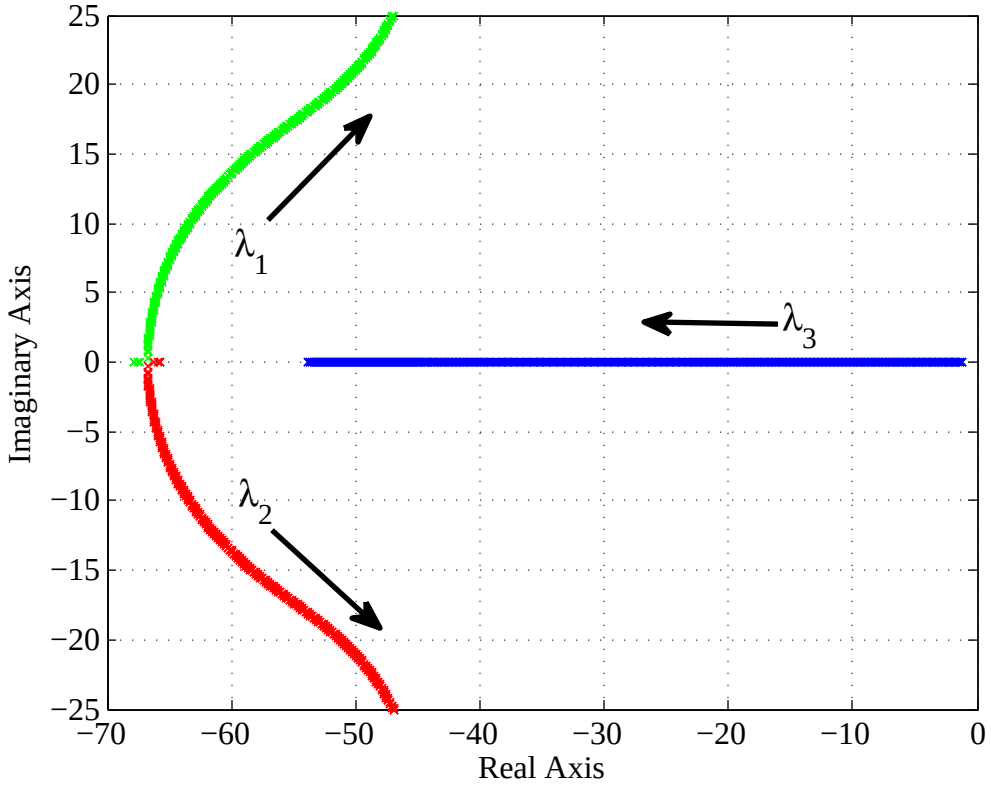

Figure 4.10: System poles trajectory for $0 < m < 1 \times 10^{-4}$, $n = 5 \times 10^{-3}$.

Fig. 4.11 shows the dynamic response of the system for the different values of frequency droop coefficient, as it can be seen by increasing this coefficient the dynamic response changes from an extreme under damped system to a critical damping system which would be much faster than the under damped system.

Fig. 4.12 shows the power angle dynamic response for different values of voltage droop coefficient,as it can be seen this coefficient does not affect the power angle and speed of the dynamic response, significantly.

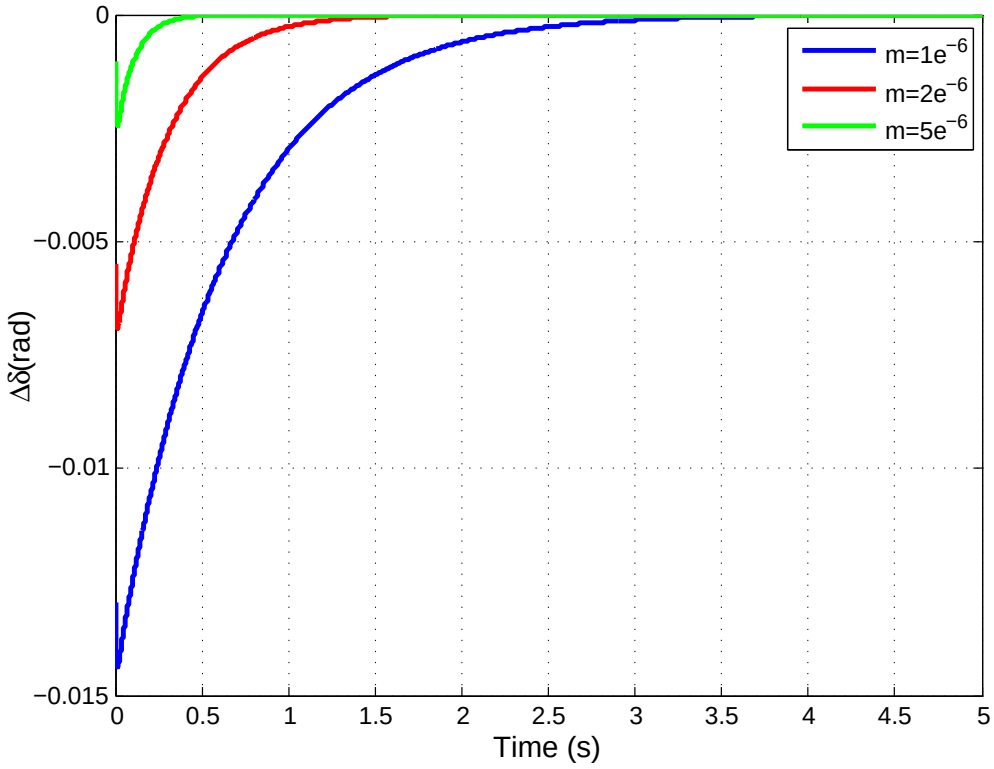

Figure 4.11: System dynamic response for switching model for different values of m ($n = 5 \times 10^{-3}$).

4.5. Simulation and Results Analysis

To evaluate the power control systems design the simulation is conducted under different scenarios for two parallel inverters. The first inverter is a grid-forming unit and the second one is controlled using combined droop and DCVC methods. Table 4.1 shows the parameters for two parallel inverters.

4.5.1. Grid-Forming Unit

In the first case, the grid-forming DG source with droop controlled inverter is studied. At $t = 1s$, the inverter is connected to from the grid and stabilize bus voltage.When the unit is connected at $t = 1s$, the droop controlled inverter raises the PCC voltage slightly above 1 per unit (Fig. 4.13) and the frequency is maintained at $60Hz$ (Fig. 4.14). At $t = 5s$ when a load is connected to the PCC, both frequency and PCC bus voltage drop based on the droop control coefficient while the converter output active and reactive powers increase to

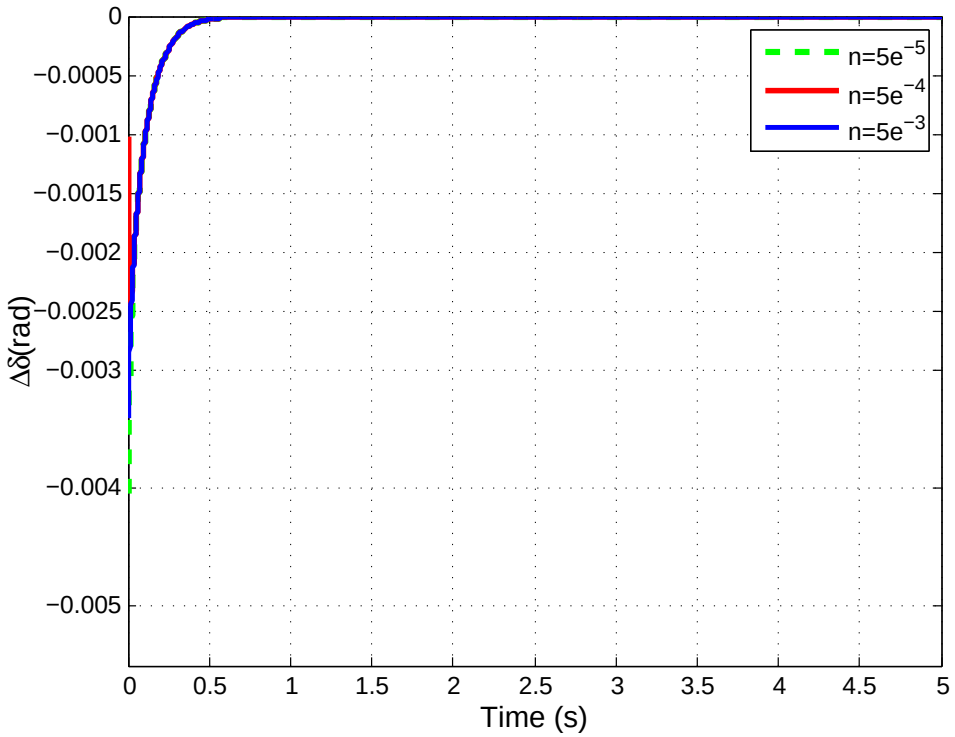

Figure 4.12: Power angle dynamic response for different values of n ($m = 5 \times 10^{-6}$).

meet the load demand (Fig. 4.15). Also, the three-phase current changes from 0A to about $50A$ (amplitude) with a good power quality (Fig. 4.16).

4.5.2. Parallel Connected Inverters Under Equal and Unequal Sharing

In the second case, the distributed ac power supply system with the droop and DCVC controlled inverters is studied for equal active power sharing with an R/X ratio of 0.13 for the distribution lines connecting the two units. The droop controlled inverter and first RL are connected to the PCC at $t = 1s$ and the DCVC controlled inverter is connected to the PCC at $t = 3s$. For the DCVC controlled inverter, only zero and generating reactive power is allowed. As a result, the bus voltages at PCC1 and PCC2 are slightly higher than 1 per unit before $t = 1s$ and the frequency is $60Hz$ (Fig. 4.17 and Fig. 4.18). When at $t = 3s$ the DCVC controlled inverter is connected, the load is shared equally between two units and the bus voltages are regulated to 1 per unit. When the second RL load is connected to the PCC at $t = 7s$, there is a frequency drop caused by the load demand. The frequency

Table 4.1: Parameters for parallel inverters structure.

System Parameters	Inverter #1	Inverter #2
Inverter rated capacity (KVA)	100	100
Inductor filter (mH)	2.5	1
Inductor ESR (Ω)	0.1	0.06
Capacitor filter (μF)	100	100
Line inductance (mH)	0.154	0.154
Line resistance (Ω)	0.076	0.076
DC voltage (V_{dc}) (V)	1200	1200
Switching frequency (KHz)	6	6
Line-line rms voltage (V)	690	690
Nominal frequency (Hz)	60	60
Frequency droop coefficient (equal sharing)	5×10^{-6}	5×10^{-6}
Frequency droop coefficient (unequal sharing)	5×10^{-6}	10×10^{-6}
Voltage droop coefficient	5×10^{-3}	-

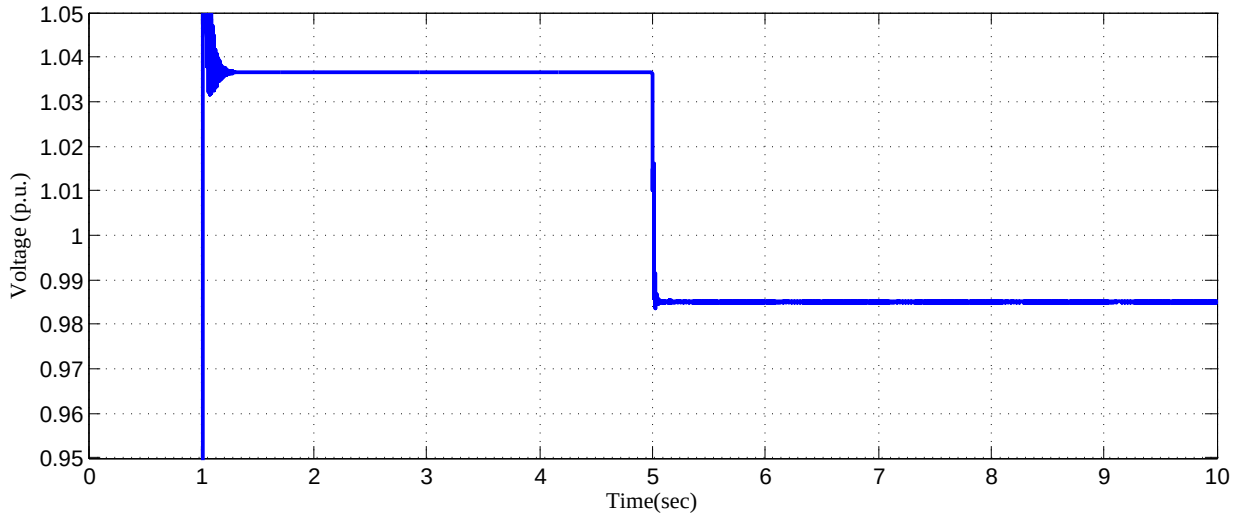

Figure 4.13: *ac*-bus voltage.

deviation causes a power sharing control between the conventional droop controlled inverter and DCVC controlled inverter according to the equal droop coefficients defined in Table 1 for the two parallel inverters. As shown in Fig. 4.19, the active powers are shared equally between the two units. Unlike conventional parallel inverters control in islanded mode, the reactive power droop control is not needed. The reactive power of the second unit is automatically determined to maintain the stability of PCC2 voltage while the rest reactive

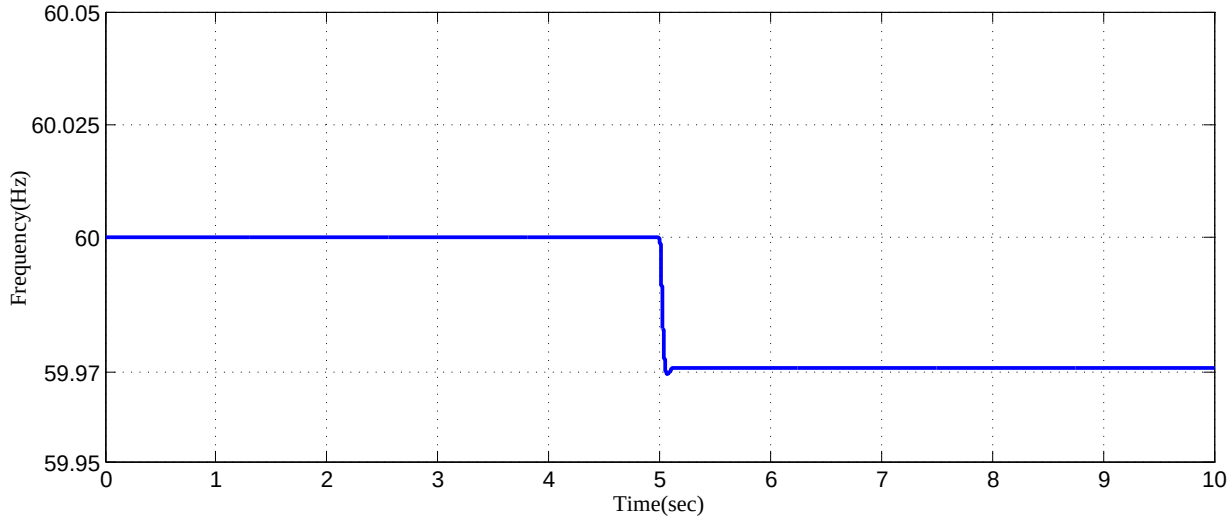

Figure 4.14: *ac*-bus frequency.

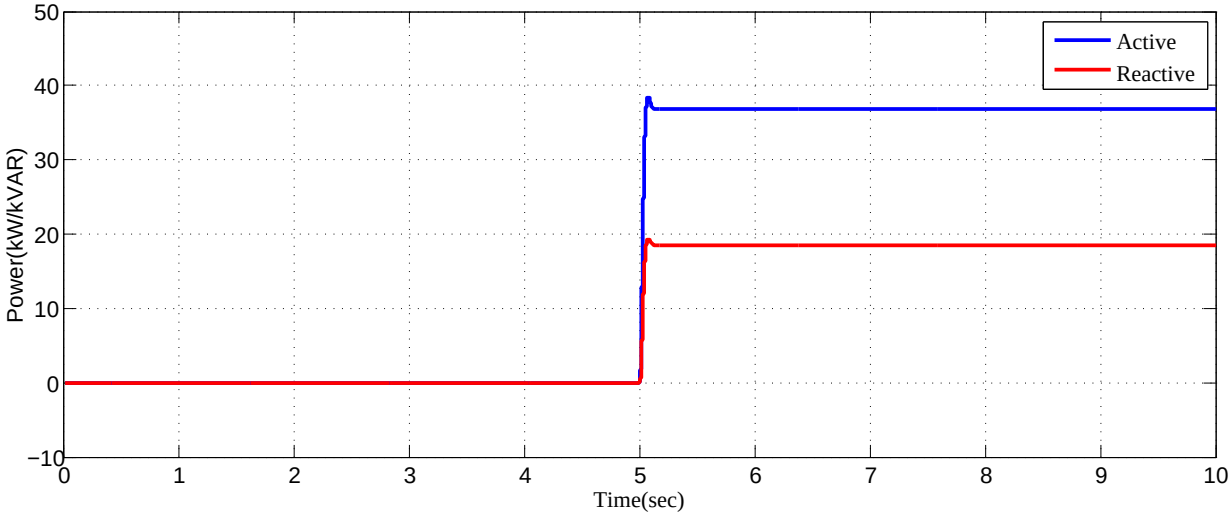

Figure 4.15: Active and reactive power at PCC1.

power demand is met by the first unit. As it can be seen from Fig. 4.17, the system voltage is reliable at both PCC1 and PCC2 for the low R/X ratio of the distribution lines. When the third RL load is connected to the PCC at $t = 11s$, there is a further frequency drop caused by the load demand (Fig. 4.18). Similarly, the active power is equally shared and the reactive power is determined by the combined DCVC and droop controllers to maintain the PCC voltage around 1 per unit. Overall, the performance evaluation demonstrates great

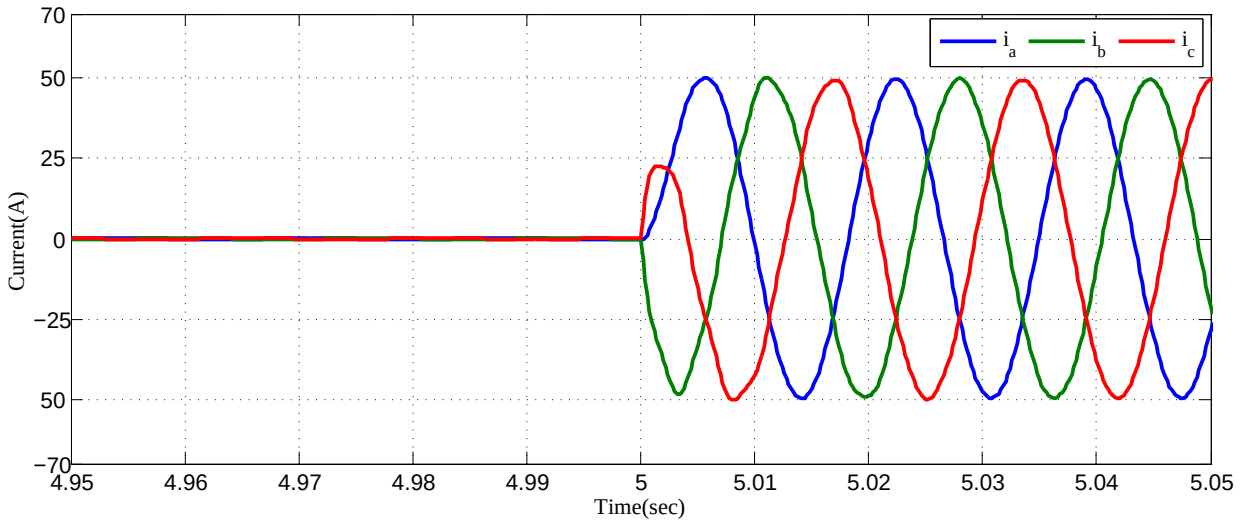

Figure 4.16: Three-phase current at PCC1.

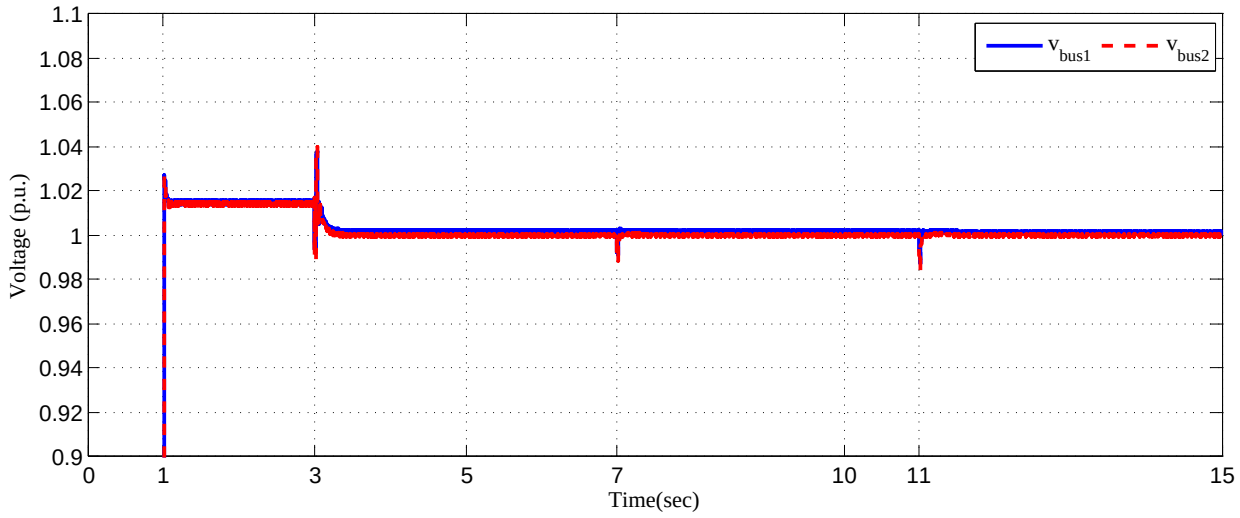

Figure 4.17: Bus voltage at PCC1 and PCC2.

advantages of the proposed droop and DCVC control technique for the distributed *ac* power supply system.

The third case study according to the unequal droop coefficients defined in Table 1 for the two parallel inverters. As shown in Fig. 4.21, the bus voltage at PCC1 and PCC2 is regulated to 1 per unit when the DCVC controlled inverter is connected to the PCC. The frequency and bus voltage control is satisfactory as case 2. The active powers of the two

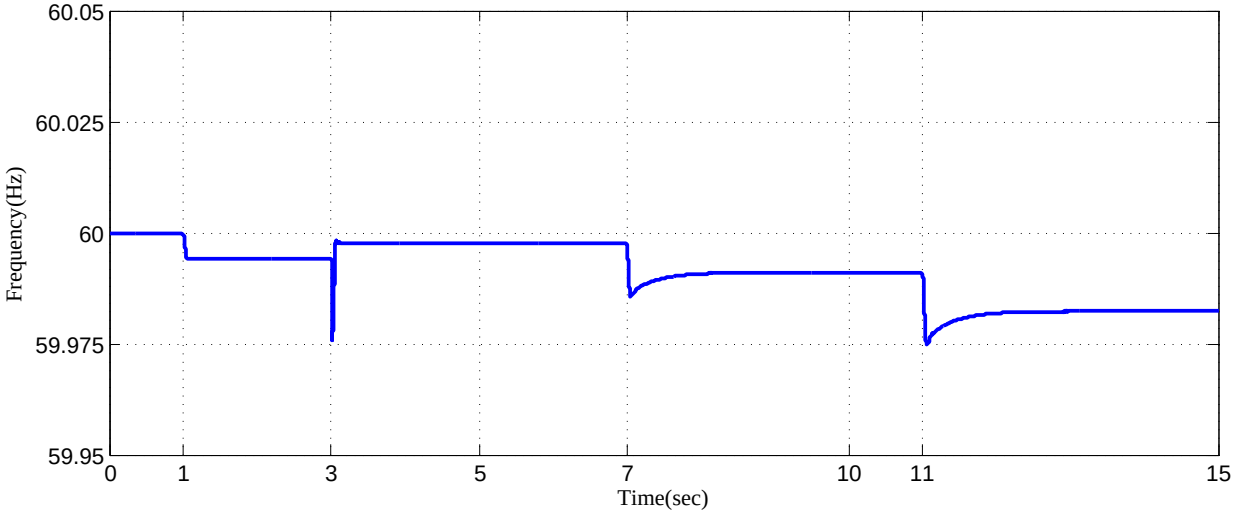

Figure 4.18: *ac*-bus frequency.

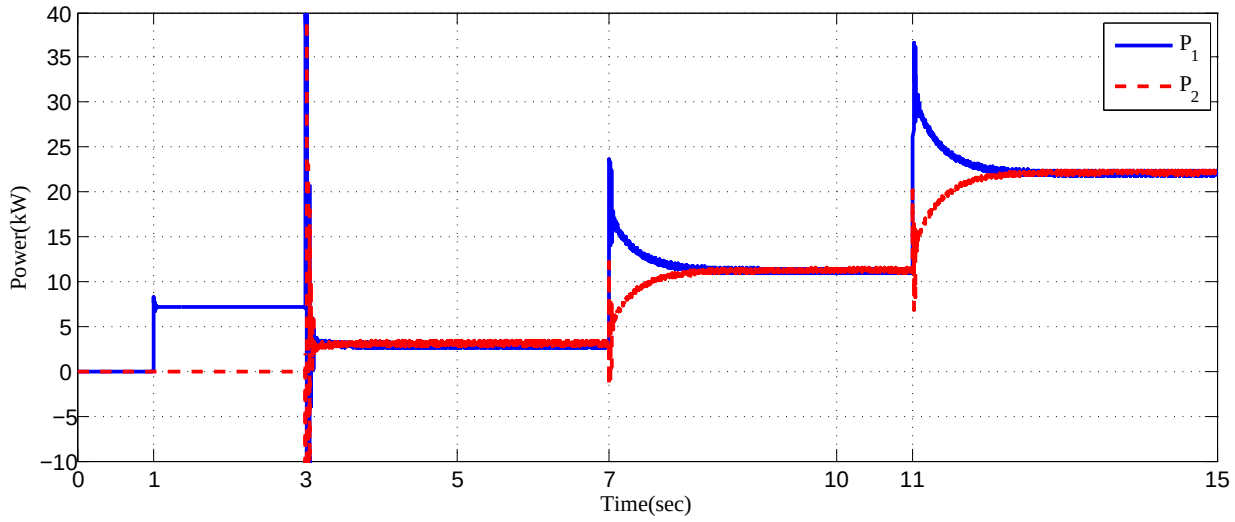

Figure 4.19: Active power at PCC1 and PCC2.

units are shared exactly according to predetermined droop coefficients between the two units as it can be seen in Fig. refP3. While reactive power is also shared between two units to regulate the PCC voltage.

4.6. Experimental Verification

To evaluate the proposed control system design and analysis an experiment is conducted for a grid-forming inverter connected in parallel with a DCVC controlled inverter.

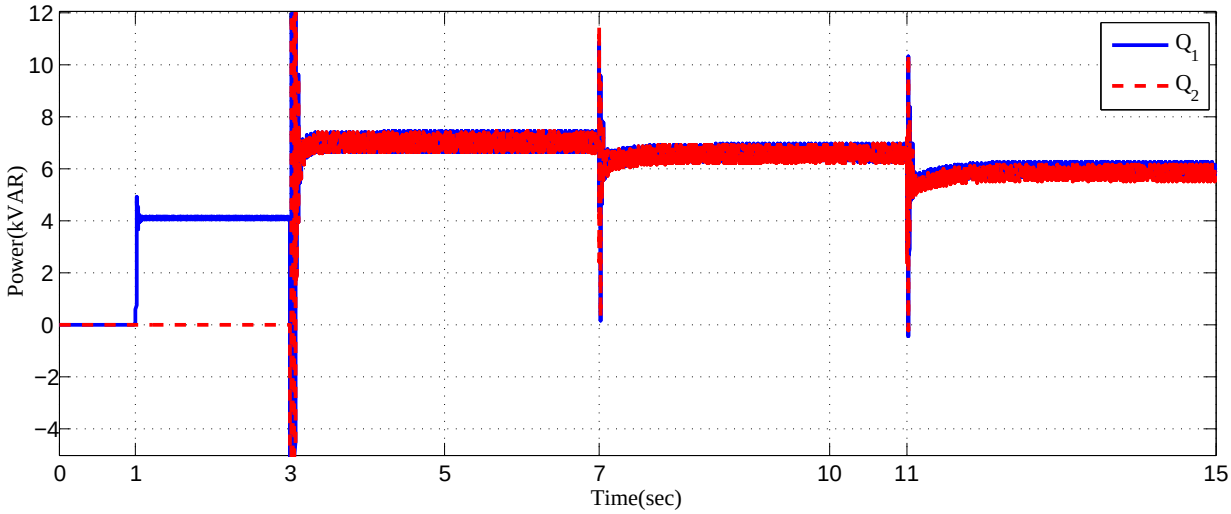

Figure 4.20: Reactive power at PCC1 and PCC2.

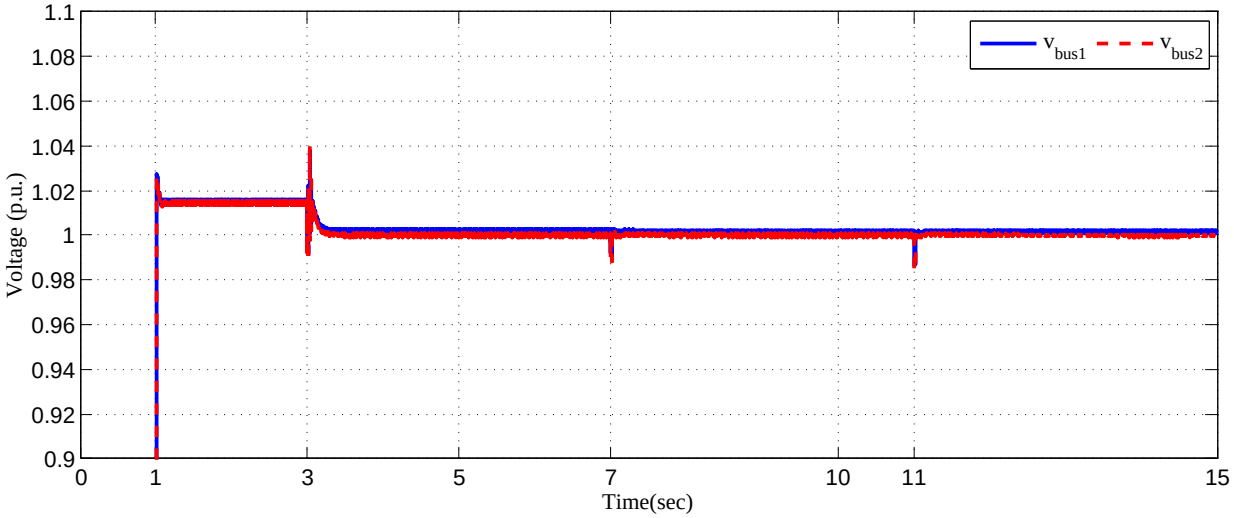

Figure 4.21: Bus voltage at PCC1 and PCC2.

Table 4.2 summarizes the hardware and controller parameters using in experiment. Fig. 4.25 shows the hardware setup, as there are two three-phase inverters two separate *dSPACE 1103* systems are used for conducting the experiment.

We assumed two DG sources are of the same capacity, each of which is implemented using a separate DC power source. Fig. 4.27 shows the active power sharing between the two units. At $t = 0s$, the grid forming unit is connected and all the load is supplied by this

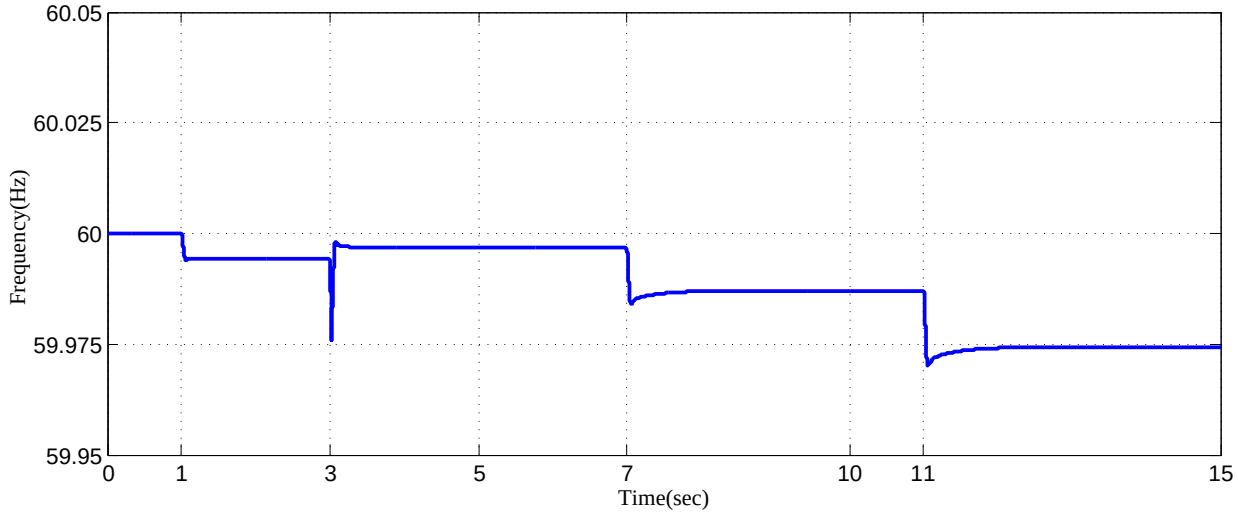

Figure 4.22: *ac*-bus frequency.

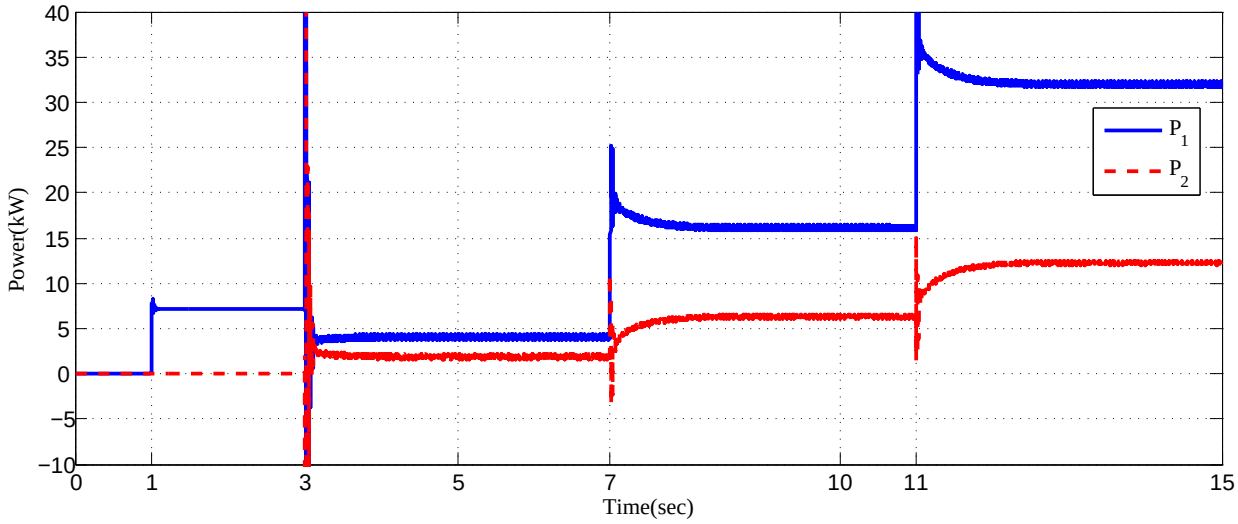

Figure 4.23: Active power at PCC1 and PCC2.

unit, while forming the PCC bus voltage as shown in Fig. 4.28. At $t = 21s$, the second unit is connected and as shown in Fig. 4.27 the load is shared between two units equally. At $t = 55.5s$ when there is a load increase, both units react to the load change and share the total load equally. Fig. 4.26 shows the *ac* bus frequency and it is shown that the frequency remains in the limit even when load changes sharply at $t = 55.5s$. As it can be seen in Fig. 4.28 and 4.29, the bus voltage maintained at 1 p.u. at PCC1 and PCC2.

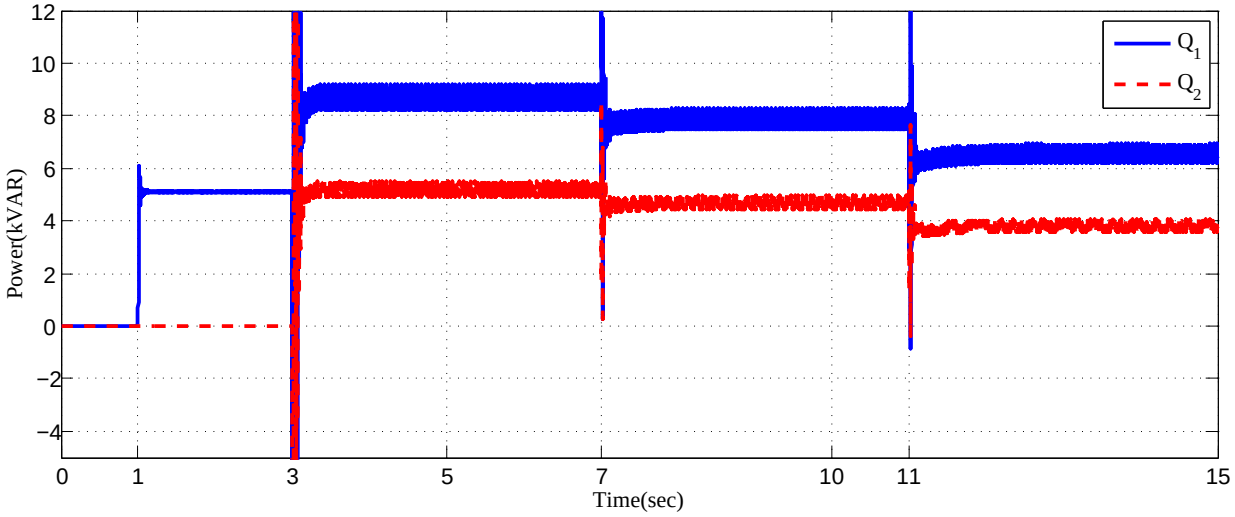

Figure 4.24: Reactive power at PCC1 and PCC2.

Table 4.2: Experimental parameters for parallel connected inverters.

System Parameters	Inverter #1	Inverter #2
Inverter rated capacity (VA)	0.5×10^3	0.5×10^3
Inductor filter (mH)	1.5	1.5
Inductor ESR (Ω)	0.364	0.364
Capacitor filter (μF)	5	5
DC voltage (V_{dc}) (V)	120	120
Switching frequency (KHz)	12	12
Line-line rms voltage (V)	61.24	61.24
Nominal frequency (Hz)	60	60
Frequency droop coefficient (equal sharing)	5×10^{-3}	5×10^{-3}
Voltage droop coefficient	1×10^{-4}	-

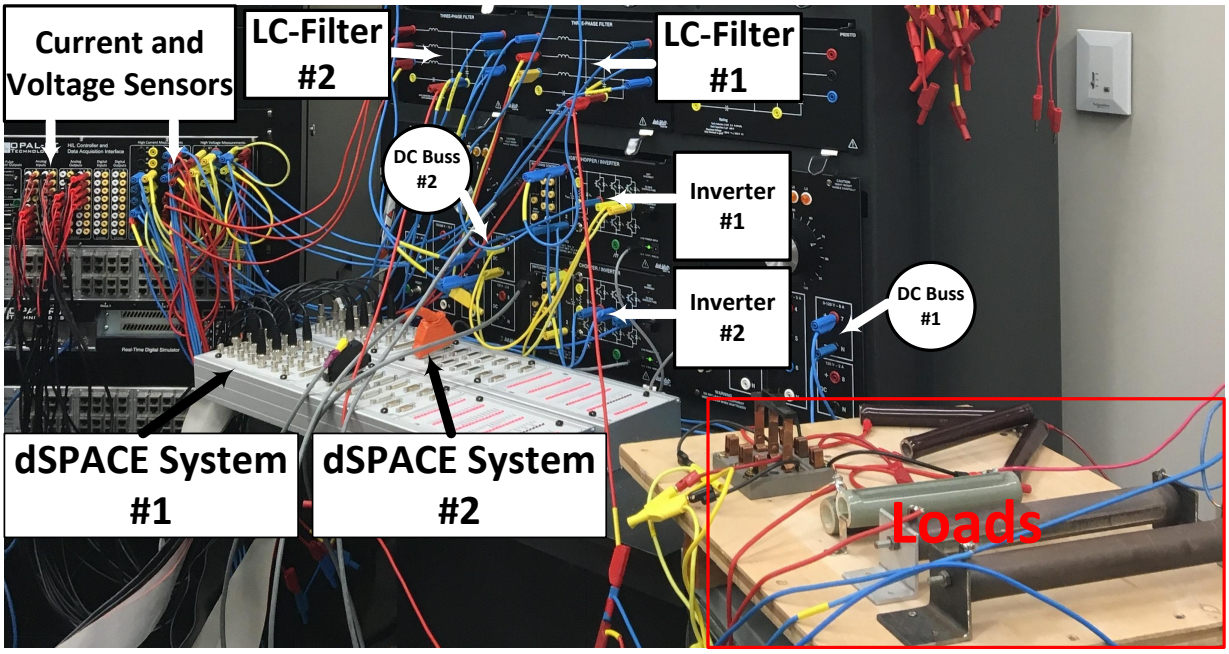

Figure 4.25: Experiment Setup.

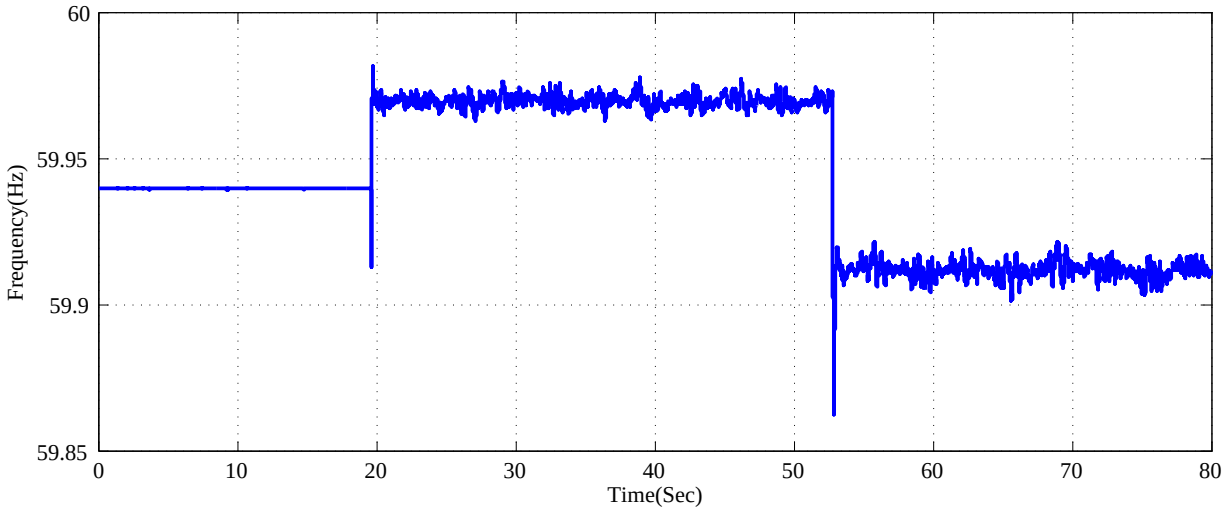

Figure 4.26: Frequency at *ac* bus.

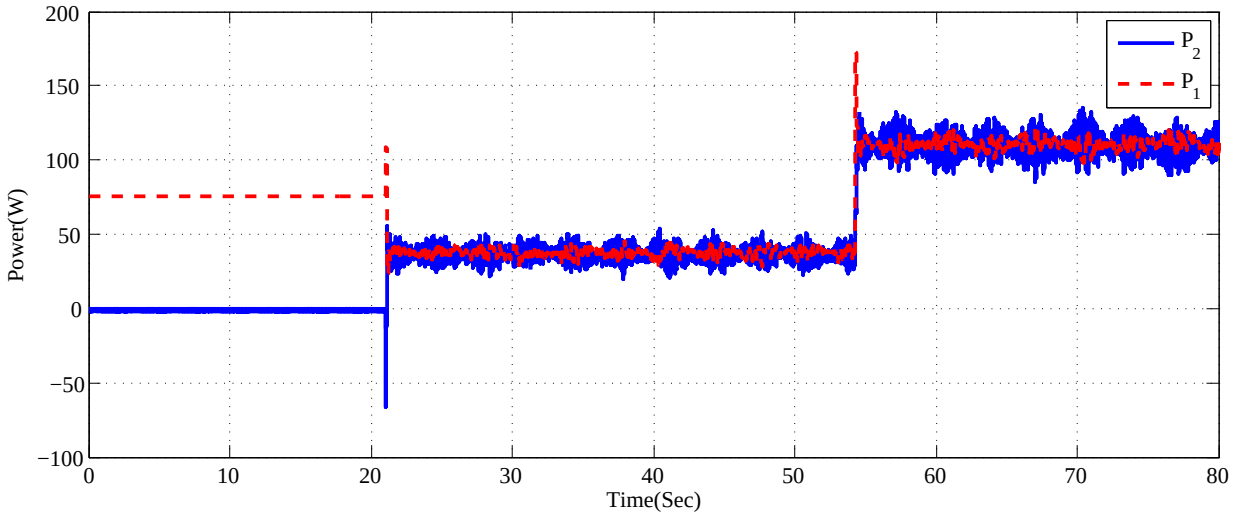

Figure 4.27: Active power sharing between two units.

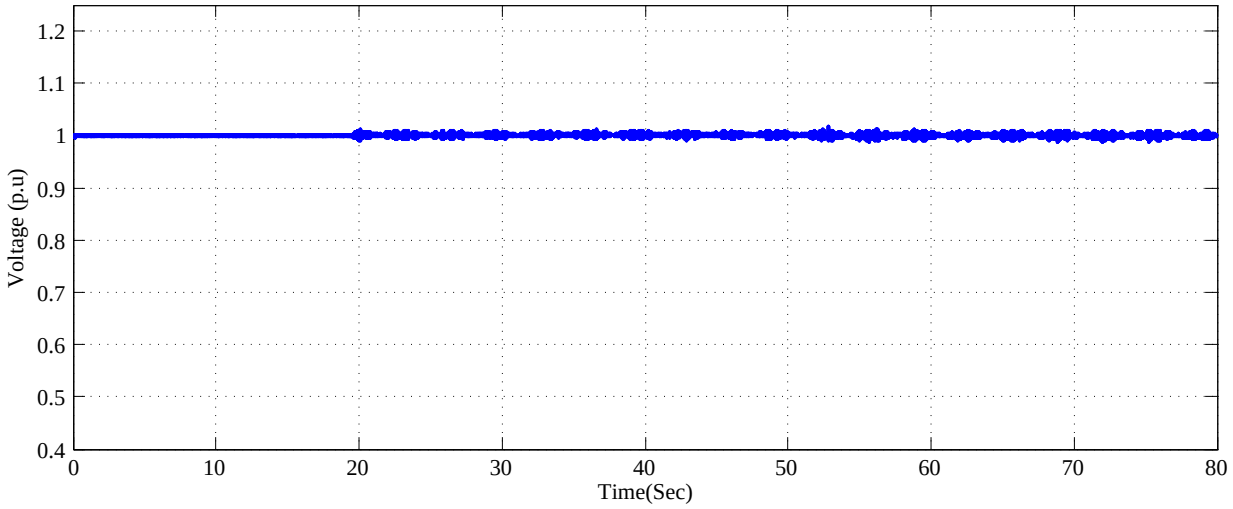

Figure 4.28: Bus voltage at PCC1.

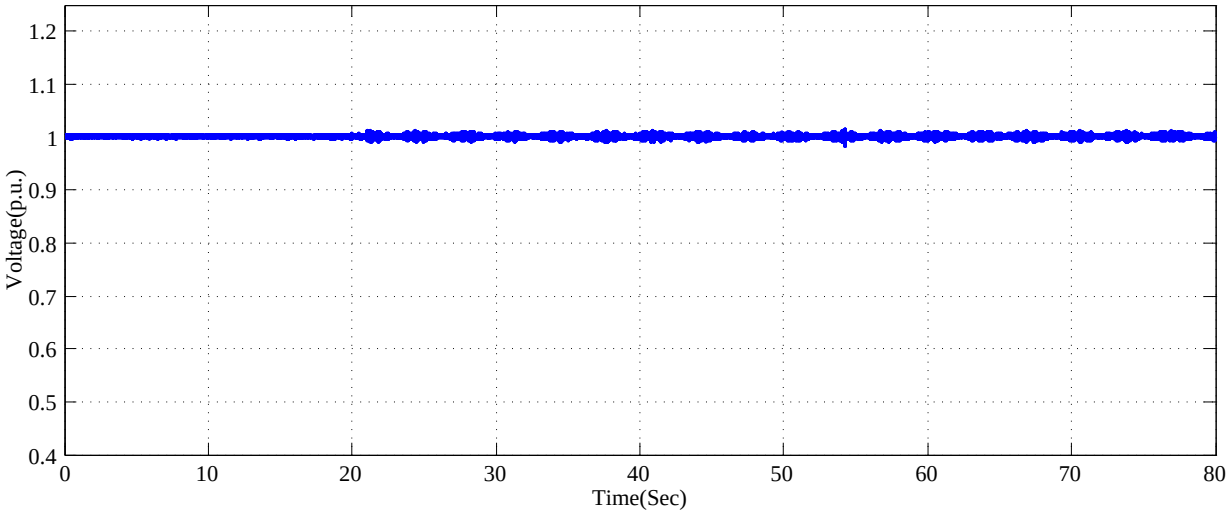

Figure 4.29: Bus voltage at PCC2.

Chapter 4 References

[1] Josep M Guerrero, José Matas, L Garcia De Vicunagarcia De Vicuna, Miguel Castilla, and Jaume Miret. Wireless-control strategy for parallel operation of distributed-generation inverters. IEEE Transactions on Industrial Electronics, 53(5):1461–1470, 2006.

[2] Wei Yao, Min Chen, José Matas, Josep M Guerrero, and Zhao-Ming Qian. Design and analysis of the droop control method for parallel inverters considering the impact of the complex impedance on the power sharing. IEEE Transactions on Industrial Electronics, 58(2):576–588, 2011.

[3] Jinwei He and Yun Wei Li. Analysis, design, and implementation of virtual impedance for power electronics interfaced distributed generation. IEEE Transactions on Industry Applications, 47(6):2525–2538, 2011.

[4] Karel De Brabandere, Bruno Bolsens, Jeroen Van den Keybus, Achim Woyte, Johan Driesen, and Ronnie Belmans. A voltage and frequency droop control method for parallel inverters. IEEE Transactions on Power Electronics, 22(4):1107–1115, 2007.

[5] Allen J Wood and Bruce F Wollenberg. Power generation, operation, and control. John Wiley & Sons, 2012.

[6] Hua Han, Xiaochao Hou, Jian Yang, Jifa Wu, Mei Su, and Josep M Guerrero. Review of power sharing control strategies for islanding operation of ac microgrids. IEEE Transactions on Smart Grid, 7(1):200–215, 2016.

[7] Malek Ramezani, Shuhui Li, and Yang Sun. Combining droop and direct current vector control for control of parallel inverters in microgrid. IET Renewable Power Generation, 0(pp), 2016.

[8] Mehdi Savaghebi, Alireza Jalilian, Juan C Vasquez, and Josep M Guerrero. Secondary control for voltage quality enhancement in microgrids. IEEE Transactions on Smart Grid, 3(4):1893–1902, 2012.

[9] Ernane Antônio Alves Coelho, Dan Wu, Josep M Guerrero, Juan C Vasquez, Tomislav Dragičević, Čedomir Stefanović, and Petar Popovski. Small-signal analysis of the microgrid secondary control considering a communication time delay. IEEE Transactions on Industrial Electronics, 63(10):6257–6269, 2016.

5. CONCLUSIONS AND FUTURE WORK

5.1. Conclusion

In this thesis the power control of parallel inverters in a distributed AC power supply system is investigated. In power control system design the main assumption is based on the lack of the possibility for control signals communication between different units. Therefore, the droop technique is the base for power control system design. To mitigate the shortages associated with droop method, such as voltage drop and reactive power sharing in the case of imbalance transmission lines, the DCVC based control technique is integrated with droop method. In the first chapter of this thesis, which is the introduction, the different methods applying to the power control of the parallel inverters are presented and pros and cons of each method are investigated. The power control system design are provided in the next chapters. The overall control system includes different parts as follow.

- The first part and the most inner loops of the nested control loops system is the current and voltage control loops for controlling the power of each unit and then sharing the power between inverters. The Second chapter of this thesis presented the current and voltage control loops design for a VSI, and it is shown that the control system with inductor current and capacitor voltage feedbacks impose an inductive impedance on the output of the inverter.
- Although, the droop technique benefits from being a wireless control system, there are some weaknesses inherent in this technique. One of this technique is the voltage drop held by reactive power control, and the other one is being sensitive to transmission lines impedance. The integration of the DCVC based method, which is presented in chapter two, with droop method overcomes this shortages in droop technique.

- To integrate the DCVC based unit there is a need to a stable grid voltage; therefore, a grid forming unit, which is controlled based on the conventional droop method, is designed and used to stabilize the bus voltage.
- In distributed AC power supply systems the secondary and tertiary control levels are also applied to control the system. In islanding mode which is investigated in this thesis the highest control level is the secondary control. A droop based secondary control level is also integrated with primary control level in this thesis to receiving the control command from the control center of the system and sharing the power accordingly.

5.2. Future Work

Integrating the DCVC with droop control needs a grid forming unit; therefore, one of the future work could be to investigate how to apply the DCVC technique to a stand alone VSI. The islanding mode is investigated in this thesis; hence, the grid-connected mode and the transition between these two modes could be an appropriate research for continuing of this research. In grid-connected mode integrating the tertiary control level to primary and secondary control levels can be investigated as well.